SIEMENS

Vol. 8 · No. 1 · 2001

MAGNETOM Flash

An Applications Reference for Siemens MAGNETOM Users

:MRI in Pediatric Radiology – Possibilities and Limitations of Low Field Magnetic Resonance Imaging:

M. Wagner, P. Kreissler[1], R. Kuth[1], T. Rupprecht

Department of Pediatric Radiology
Hospital and Outpatient Clinic for Children and Adolescents
(Professor Dr. W. Rascher, Director)
Friedrich-Alexander University, Erlangen-Nuremberg

[1] Siemens Medical Engineering, MR Research and Development, Erlangen, Germany

Abstract:

MRI has been used in pediatric imaging for several years. It provides excellent anatomic detail and tissue characterization combined with the advantage that it is not associated with the application of ionizing radiation to the radiation sensitive infant organism. Low field MRI provides some additional advantages like a lower rate of sedations, easier monitoring of sedated patients and the option of interventional examination and therapy. The disadvantages, however, are the slightly prolonged examination times and the lower signal-to-noise ratio compared to high-field MR scanners. In the future, new techniques using modern gradient echo sequences will provide fast imaging methods with a very high signal-to-noise ratio which

continuation next page

Technical Characteristics –
Monitoring and Sedation of Patients –
Possible Interventions –
Disadvantages in Comparison to High-Field Magnetic Resonance Systems –
Fields of Application –
Typical Diagnoses –
Prospects and Perspectives

** Prior to 3 weeks out of the body, infant imaging is not determined to be safe.*

:In this issue:

continuation from title

could partially replace conventional x-ray imaging. In the presented article we report our experiences in low-field MR imaging of pediatric patients. The possibilities as well as the limitations of this imaging modality are pointed out.

Keywords: MRI, low-field MRI, children, sedation and monitoring.

Introduction

Magnetic resonance imaging is an imaging modality free of ionizing radiation. For this reason, especially in pediatric patients*, it is frequently applied. The development of low-field magnetic resonance imaging systems in recent years has opened up new avenues for the use of diagnostic MR imaging in pediatric radiology. On the one hand, magnetic resonance imaging using field strengths of around 0.2 Tesla (T) is subject to physical limitations compared to traditional high-field magnetic resonance technology; on the other hand, though, the different construction of these systems (open design) results in improved opportunities for patient monitoring and new possibilities for interventional procedures.

From the Editor

Change of address? Would you like to be added to our mailing list?

In the US, please contact the Applications Helpline (phone 1-800-888-SIEM (7436) in the US) and give us your name and business address (no home addresses, please). MAGNETOM Flash is distributed outside the US by local Siemens offices. Please contact me and I will make sure that you are included on your local support office's distribution list.

We hope you will find the information in this issue of MAGNETOM Flash helpful.

Dagmar Thomsik-Schroepfer, Editor

For the last two-and-a-half years, an open low-field magnetic resonance system from Siemens (MAGNETOM Open) has been installed in the Hospital and Outpatient Clinic for Children and Adolescents at Erlangen-Nuremberg University. This paper is a presentation of our experiences using this method as well as a collection of interesting patients.

Opportunities and Limitations of Open Magnetic Resonance in the "Routine" Examinations

We have examined approximately 1500 children in the last two and a half years using magnetic resonance imaging (MRI). Approximately 80 % of these examinations involved indications in the central nervous system (CNS); 15% involved thoracic diseases, diseases of the abdomen, and diseases of the musculo-skeletal system; finally, 5 % of these examinations involved congenital heart defects.

In the following, we present a selection of typical diagnoses for each individual group of examination indications, and discuss the opportunities and limitations of the method.

Examinations of CNS

Magnetic resonance imaging is a standard diagnostic technique for the CNS (1,2). In pediatric medicine, it is used in the case of congenital diseases (deformities in the brain or spinal cord [figs. 1-3], metabolic defects [4]); for tumor location; for follow-up of tumors [5], hydrocephalus, and chronic inflammatory diseases [6]; as an imaging technique in cases of convulsions [7] or equivocal neurological symptoms; and in the diagnosis of infarctions or hemorrhage [8]. Figures 1-9 present a range of typical diagnostic situations.

All customary examination procedures for the CNS area are also available in low-field magnetic resonance tomography. In some cases, the inferior signal-to-noise ratio due to physical constraints results in a slight increase in examination time over that required for a high-field examination. As figs. 1, 4 and 9 demonstrate, inversion recovery (IR) sequences are outstandingly well suited to improve and clear imaging of gyration. At the present time, image quality in angiography sequences [figs. 1, 8, 9] is still inferior to that obtainable in a high-field system. In case of doubt, the MR tomography results should be verified using color Doppler sonography and quantified by pulsed Doppler sonography [figure 1].

Currently, the principal technical limitation on low-field MRI in the CNS area is in imaging very thin slices. Slice thicknesses of 1-2 mm, which we and many other institutions use for planning surgical interventions for epilepsy, can be successfully achieved using 3D sequences. Images can be reconstructed with a slice thickness of 2 mm when a Fast Low-Angle Shot (FLASH) 3D examination is conducted. The datasets are obtained in a way suitable for image fusion using single-photon emission computed tomography (SPECT) and magnetic encephalography (MEG) examinations [figure 10].

As a result of the inferior signal-to-noise ratio, currently neither functional MR sequences nor spectroscopy can be realized on low-field magnetic resonance systems. At the moment, this is the only real limitation on this examination method in the field of pediatric CNS diagnosis.

Cardiac and Thoracic Examinations

MRI has been a standard technique for some years now in the diagnostic imaging of the thorax and anomalies of the great vessels (3-5). But it is also possible using this technology to produce good quality images of congenital cardiac defects and anomalies in the thoracic venous course, as well as anomalies in the area of the trachea (6-9).

Finally, there are textural anomalies of the myocardium (arrhythmogenic right ventricle) that can be diagnosed almost exclusively with MRI (10). Here, T1-weighted spin echo sequences in all 3 orientations (axial, coronal, sagittal) are chiefly used. In addition, double oblique sequences are used for imaging of the course of the aorta.

In recent years, we have examined 5 children whose severe ventricular arrhythmias led clinically and electrocardiographically to the suspicion of an arrhythmogenic right ventricle. This suspicion was confirmed in three of the children by means of a cardiac low-field magnetic resonance examination.

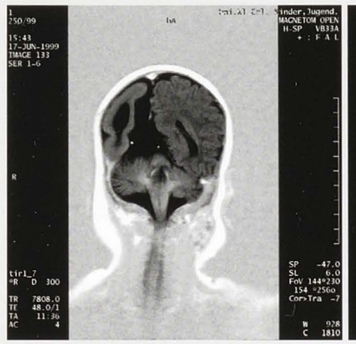

Fig. 1a

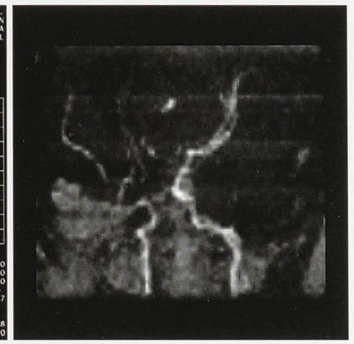

Fig. 1b

Figure 1a: Two-month-old boy with congenital malformation of the right cerebral hemisphere which is lisencephalic and smaller than the left hemisphere which appears normal.

Figure 1b: MR angiography of the same patient revealed a missing lenticulostriate artery which was confirmed by Doppler sonography. Additionally, the right anterior cerebral artery was missing in this patient. If the malformation was the result of an early intrauterine infarction or caused by a primary malformation of the arteries is not known. The quality of MR angiography is poorer compared to high-field imaging and is even more difficult to interpret in this patient, due to small size of the anatomic structures.

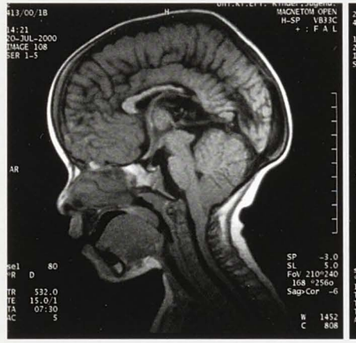

Fig. 2a

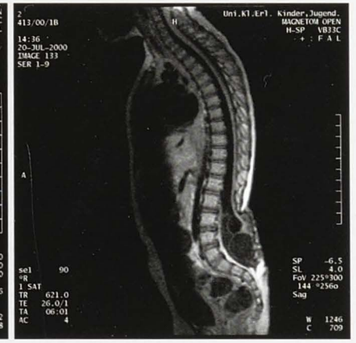

Fig. 2b

Figure 2a: T1-weighted image of a two-year-old girl with postoperative spina bifida and Chiari II malformation. The typical features of the malformation are seen in the medial sagittal plane. Low posterior fossa contents with herniated tonsils and elongated fourth ventricle, partial agenesis of the corpus callosum as well as polymicrogyria, a large massa intermedia and the beaking of the tectum are characteristics of this malformation.

Figure 2b: Midsagittal T1-weighted spin echo of the spine in the same patient. The large lumbar defect is easily depicted. The spinal cord is fixed to the operation site indicating a tethered cord which in this patient had become symptomatic in terms of a decrease of the motor function of the left leg. Additionally, two arachnoid cysts are noted at the lower end of the spinal cord.

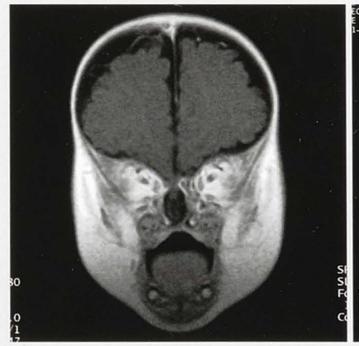

Fig. 3a

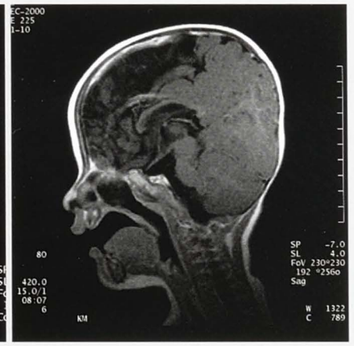

Fig. 3b

Figure 3a: Eleven-month-old patient with frontal encephalocele. The T1-weighted coronal spin echo revealed a small cele within the nasal cavity. The intracranial connection is clearly depicted. Note the wide arachnoid space which is considered normal in the young child.

Figure 3b: Sagittal T1-weighted spin echo sequence of the same patient. The encephalocele is seen very softly within the nasopharynx, occluding most of the right upper airway.

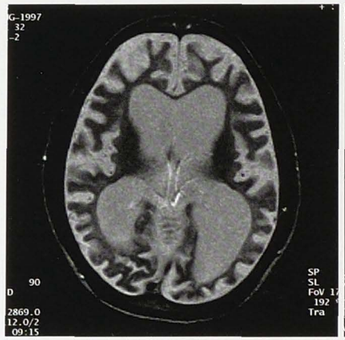

Fig. 4a

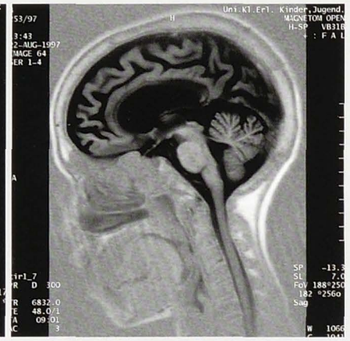

Fig. 4b

Figure 4a: 14 year-old girl with mucopolysaccharidosis III (Sanfilippo) and severe physical and mental retardation. Axial T2-weighted spin echo shows dilated ventricles and severe atrophy of the brain.

Figure 4b: Sagittal IR sequence of the same patient. The atrophy is easily depicted. Most of the white matter is destroyed in this patient secondary to the underlying disease. However, exact differentiation of the white and gray matter is no longer possible in this patient.

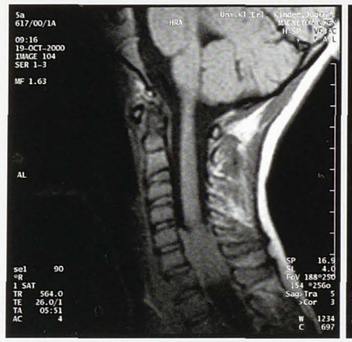

Fig. 5a

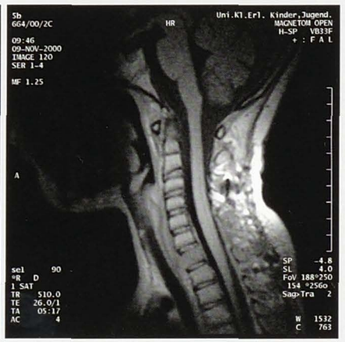

Fig. 5b

Figure 5a: Sagittal T1-weighted spin echo of a seven year-old patient presenting with upper extremity paresis. The image shows an intraspinal tumor over 3 cervical segments. Partial destruction of the seventh cervical vertebra is present.

Figure 5b: Postoperative T1 weighted spin echo of the same patient. No residual tumor is seen within the spinal canal. A fine syrinx is observed as well as a persistent spinal edema causing a mild thickening of the spinal cord. Note the scarring and the partial resection of the spinous processes at the operation site.
Definite histology is pending.

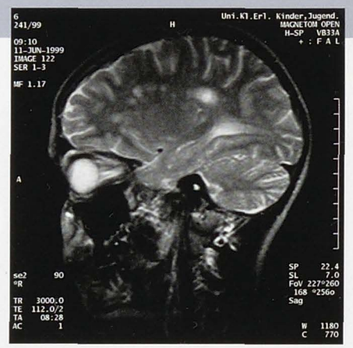

Fig. 6

Figure 6: Sagittal T2-weighted image of a 14 year-old girl suffering from cerebral involvement of systemic lupus erythematodus. The areas of cerebral vasculitis are easily depicted as regions of high signal intensity.

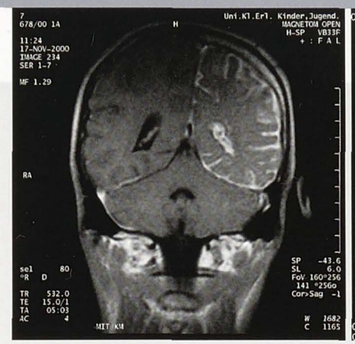

Fig. 7a

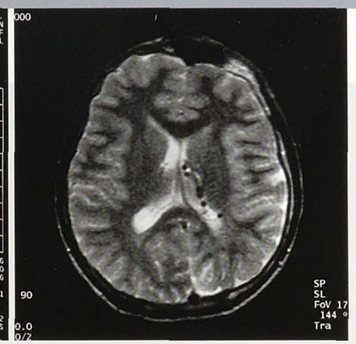

Fig. 7b

Figure 7a: 16 year-old boy with Sturge-Weber disease. Coronal T1-weighted image after contrast enhancement. Left cerebral hemiatrophy with and associated expansion of the subdural space. Cortical and meningeal contrast enhancement due to multiple vascular malformations is observed within the left hemisphere.

Figure 7b: Same patient, axial T2-weighted image. The hemiatrophy and expansion of the arachnoid space is observed in this plane as well. Note the expansion of the left frontal sinus consistent with the cerebral hemiatrophy. In addition to that, multiple enlarged vessels are seen within the left choroid plexus which were identified as veins in an additionally performed venous MR-angiography.

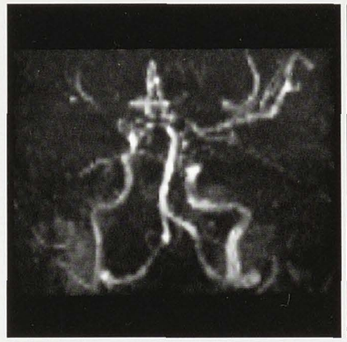

Fig. 8a

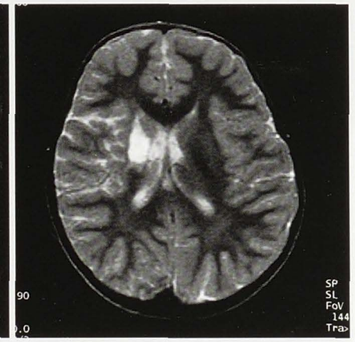

Fig. 8b

Figure 8a: Cerebral MR-angiography. Occlusion of the right middle cerebral artery (MCA) in a four-year-old girl with an infarction of the right MCA.

Figure 8b: T2-weighted spin echo sequence of the same patient. The large periventricular defect is readily apparent as well as the concomitant atrophy of the surrounding gyri.

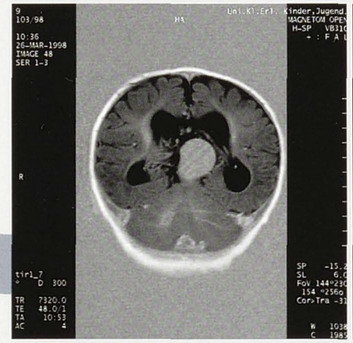

Fig. 9a

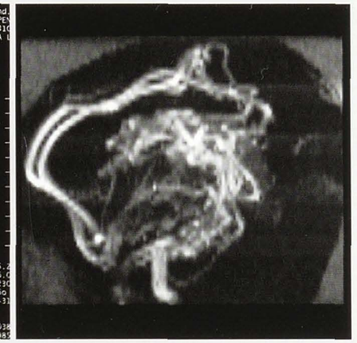

Fig. 9b

Figure 9a: Four month-old girl with large vein of Galen aneurysm following interventional angiography with coil and fibrin glue embolization of the aneurysm (Professor W. Huk, Neuroradiology, University Clinic Erlangen/Nuremberg). Coronal IR sequence. The aneurysm is easily depicted.

Figure 9b: MR-angiography, sagittal view of the same patient. The supplying vessels are clearly imaged while the aneurysm itself showed a minimal flow, indicating residual perfusion after the embolization. A complete thrombosis of the aneurysm ensued.

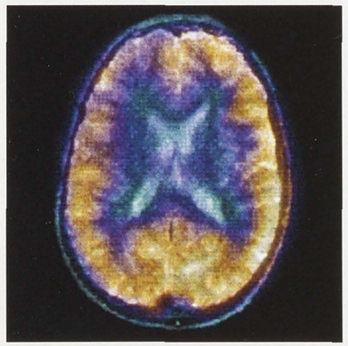

Fig. 10

Figure 10: Image fusion from a FLASH 3D examination using interictual single-photon emission computed tomography (SPECT) of a 6-year-old patient with therapy-resistant cerebral convulsive disorder associated with Rasmussen's encephalitis. The image shows a frontally reduced perfusion, with basal accentuation. The image was reconstructed in a slice thickness of 2 mm. The datasets were obtained in a way suitable for image fusion using single-photon emission computed tomography (SPECT) and magnetic encephalography (MEG) examination. (Image fusion: Dr. Platsch, Nuclear Medicine Clinic, University of Erlangen/Nuremberg).

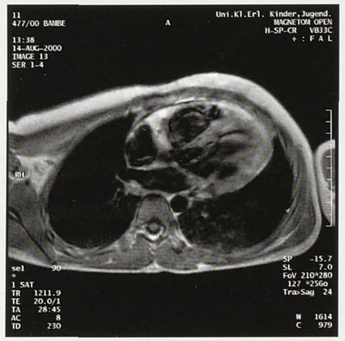

Fig. 11

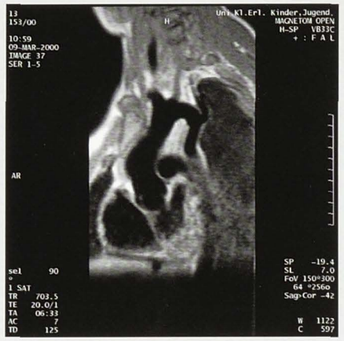

Fig. 13a

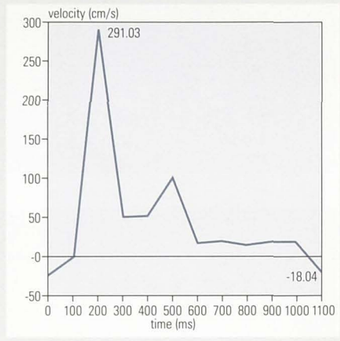

Fig. 13b

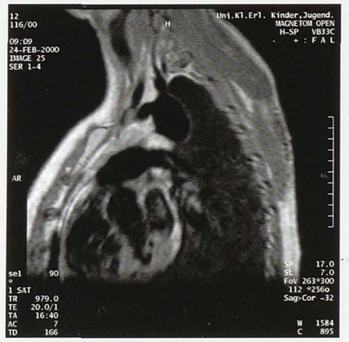

Fig. 12

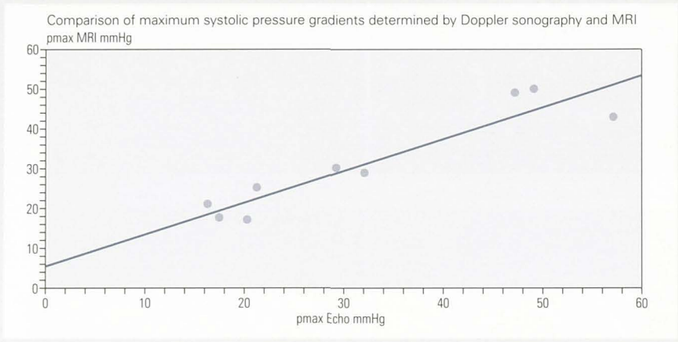

Fig. 14

Figure 11: Cardiac MR images (modified longitudinal axis with cardiac triggering) of a 12 year-old boy suffering ventricular tachycardia. The pronounced thinning of the right ventricular wall and the increased signal intensity within the right ventricular myocardium are typical evidence for fatty degeneration consistent with an arrhythmogenic right ventricle.

Figure 12: 16 year-old boy with coarctation of the aorta status post repair in his infancy. Routine follow-up MRI. Modified long axis T1-weighted spin echo with cardiac triggering. A large aneurysm of the aorta at the former operation site was diagnosed. In addition, an aneurysm of the left carotid artery was clearly depicted on the images. The patient underwent surgical repair of the aneurysms.

Figure 13a: Cardiac MRI of a 14 year-old patient status post repair of a coarctation of the aorta. The MRI revealed a hypoplastic aortic arch with prestenotic enlargement of the ascending aorta.

Figure 13b: Flow curve for the same patient. The result in the post-stenotic segment is a maximum systolic flow velocity of 291 cm/sec., which (in accordance with the modified Bernoulli equation) corresponds to a calculated pressure gradient of 34 mm Hg. A slight diastolic gradient is suggested.

Figure 14: Comparison of maximum systolic pressure gradients (pmax) for 9 patients determined by Doppler sonography and by magnetic resonance tomography. The difference between the two methods appears to be acceptable at high pressure gradients (r = 0.93, p< 0.001). The pressure gradient was calculated from the maximum flow velocities using the modified Bernoulli equation (Δpmax = 4v2).

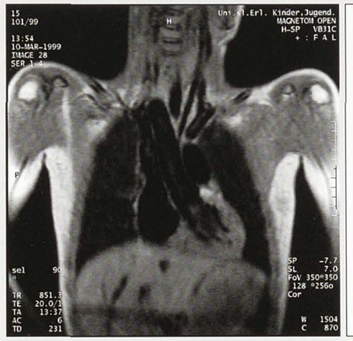

Fig. 15a

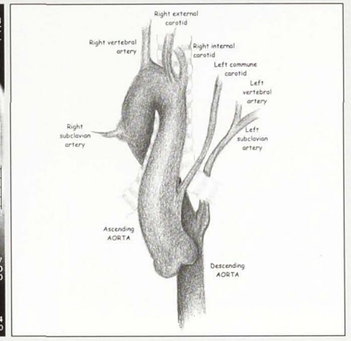

Fig. 15b

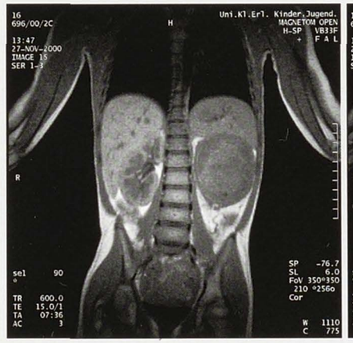

Fig. 16a

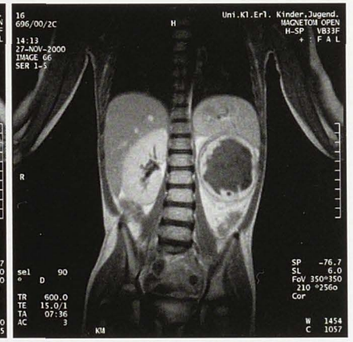

Fig. 16b

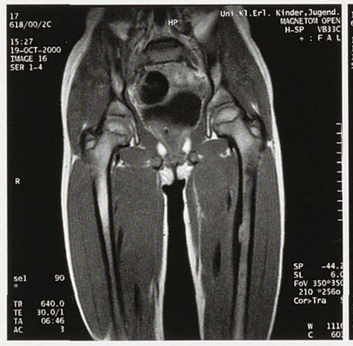

Fig. 17a

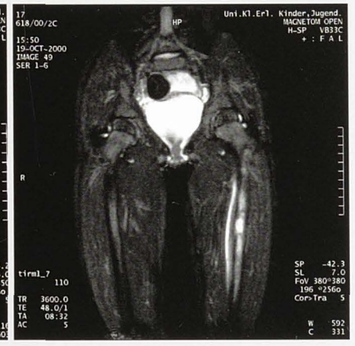

Fig. 17b

Figure 15a: Cardiac MRI in a 13 year-old girl with right cervical aortic arch. The ascending aorta is elongated and orientated to the right. The left carotid artery is easily depicted in this slice.

Figure 15b: Anatomical sketch of the right cervical aortic arch. The aortic arch is drawn up and deflected to the right. The right external and internal carotid arteries arise as independent vessels from the aortic arch; the right subclavian artery arises from an aortic diverticulum. The descending aorta intersects the central line and runs along the left side in the thoracic region. The left subclavian artery arises aberrantly from a diverticulum. (Modified from Finch MA, in: Amplatz, Moller, Radiology of Congenital Heart Disease; 1992, p. 1031).

Figure 16a: 4 ½ year-old girl presenting with a large abdominal tumor. Coronal T1-weighted image without contrast enhancement. A large left-sided abdominal mass with heterogeneous medium-signal-intensity is seen, while the left kidney could not be located.

Figure 16b: Same slice after contrast medium injection. A heterogeneous contrast enhancement was seen while the right kidney showed no pathological contrast enhancement. Histology confirmed a unilateral Wilms' tumor.

Figure 17a: 7 year-old girl presenting with swelling and pain of the left thigh. X-ray revealed a cystic process with periostal reaction. Coronal T1-weighted image without contrast enhancement. The isointense process is clearly seen within the proximal femur. Cortical thickening and periostal reaction are observed as well as an involvement of the surrounding soft tissues.

Figure 17b: Coronal fat suppressed sequence of the same patient. An increased signal intensity is noted at the site of the process as well as a bone edema involving most of the femur diaphysis and the surrounding soft tissue. Histology of the process revealed chronic osteomyelitis. Malignancy was the most important differential diagnosis and has to be excluded by histology in such cases.

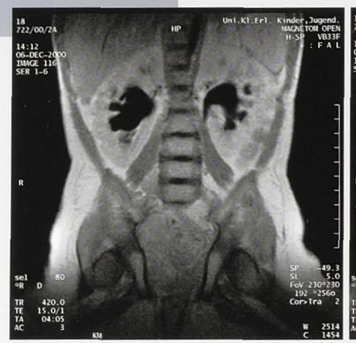

Fig. 18a

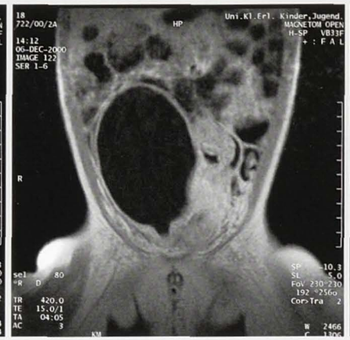

Fig. 18b

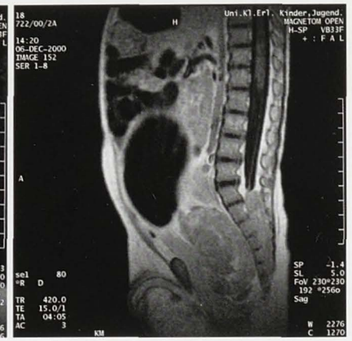

Fig. 18c

Figure 18a: Coronal T1-weighted spin echo after Gadolinium administration in an 11 month-old boy with a presacral mass of unknown origin. The mass is seen at the lower boarder of the image. Additionally, marked dilatation of both renal pelvices is noted.

Figure 18b: More anterior slice of the same patient. The bladder is dilated and shifted to the right. The bladder neck is clearly seen. The tumor compresses the urethra leading to massive urine retention in this patient. As no contrast medium is collected in the bladder during the investigation an inhibited urinary excretion may be assumed secondary to the morphological findings.

Figure 18c: Sagittal T1-weighted image after contrast enhancement of the same patient. The presacral mass is clearly seen. After contrast enhancement it showed a heterogeneous signal intensity. In the sagittal plane the intraspinal spread of the tumor is easily depicted. Histology is pending. Note the only mild motion artifacts (respiration, bowel movement) which are notably less pronounced than they would be in high-field MR imaging.

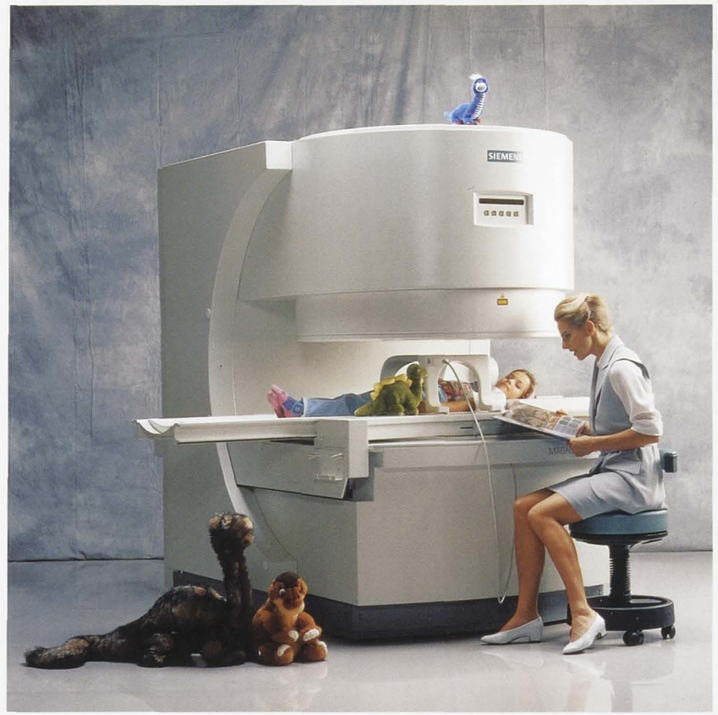

Figure 19: Typical examination of a conscious little girl. There is direct visual and physical contact with the child during the examination, which has a positive effect on the cooperation of the young patient.

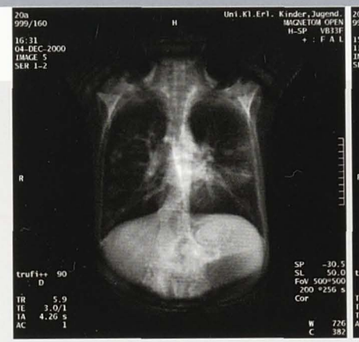

Fig. 20a

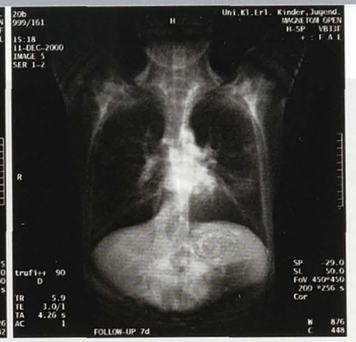

Fig. 20b

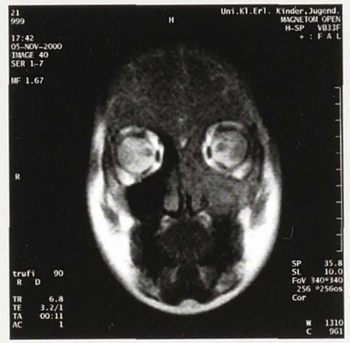

Fig. 21

Figure 20a: Fast thick-slice MRI of the lung in a 16 year-old boy with cystic fibrosis. Multiple patchy areas of increased signal are noted consistent with diffuse pneumonia. Interstitial disease is seen in its typical streaky appearance. Additionally, hilar attenuation is noted. Acquisition time for 3 slices (slice thickness 50 mm each) covering the whole thorax 3.6 sec!

Figure 20b: Follow-up of the same patient after 1 week of treatment. The pneumonic infiltrates have markedly resolved indicating the usefulness of thick-slice MRI to diagnose and later follow up acute changes in patients with chronic lung disease.

Figure 21: Fast thick-slice true FISP imaging of the paranasal sinuses in an eight year old girl presenting with fever. The left maxillary sinus is completely mucous-filled. The ethmoidal cells were involved while the sphenoid sinus was found to be free of infection. Despite antibiotic therapy the girl developed an orbital phlegmon which resolved within three days of IV antibiotic treatment. Acquisition time per slice 1.7 sec!

Fig. 11 shows as an example the cardiac low-field MR results for a twelve-year-old boy (modified longitudinal axis). In addition to electro-physiological criteria, the cardiac low-field MR diagnosis is a mainstay in diagnosing this clinical picture.

Coarctation of the aorta is the most easily imaged congenital cardiac anomaly. In our clinic, patients are regularly subjected to a follow-up MR examination after surgical repair of a coarctation in order to detect as early as possible the development of any restenosis or an aortic aneurysm. The method also enables good pre-operative aortic imaging of the morphological isthmus. In addition to the morphological image, it is also possible using MRI with the newly developed phase-sensitive flow measurement sequences to evaluate the hemodynamic relevance of the stenosis.

Figure 12 presents an aneurysm formation of the aortic arch following surgical repair of a coarctation of the aorta in a 16 year-old boy; figures 13a-b show the morphological image of a hypoplasic aortic arch and the flow curve. Figure 14 is a comparison of the pressure gradients of 9 children determined by Doppler sonography and by MRI, respectively.

As a result of the good quality image of both the vascular system and the trachea provided by MRI, anomalies of the great vessels can often be better evaluated by that technology than by angiography or bronchography.

Figure 15a shows the results for a patient whose right cervical aortic arch was diagnosed using sonography. Low-field MRI here enables easy imaging of the relationship between the bronchial and vascular structures.

Figure 15b visualizes the findings in an anatomical diagram.

Low-field MRI is also a valuable method in the field of thoracic and cardiac diagnosis; here, though, its usefulness is restricted by its somewhat inferior signal-to-noise ratio with very thin slices. Here at the Hospital and Outpatient Clinic for Children and Adolescents at the University of Erlangen, we have succeeded for the first time in establishing functional low-field MR sequences that also enable quantitative flow measurement in the region of the great vessels.

In the future, it will also be necessary to realize additional functional sequences (ejection fraction, cardiac output) for low-field diagnostics. This seems feasible in terms of the physics involved, although here too one must expect that examination times will be lengthier than they are for comparable high-field examinations.

Abdominal Examinations

The most salient feature of abdominal diagnosis in pediatric imaging is the limited degree of patient cooperation compared to adults. MRI that are customary in use with adult patients (breath-hold examinations) are of only limited practical value in pediatrics (11). This difficulty must be overcome by an optimized examination process that includes the patient's regular and even breathing (breath triggering, special sequences that perform an averaging of individual lines rather than of the entire image), and, if necessary, pharmaceutical sedation.

Figure 16 shows the examination of an infant with a central Wilms' tumor of the left kidney; figures 18a-c depict the MR results for an 11 month-old boy with a low abdominal tumor. Special line-averaged sequences for better suppression of motion artifacts due to breathing were not applied in this patient because of the even breathing during sedation.

Overall, MR diagnosis is a valuable component of pediatric abdominal imaging. Here, and especially in the case of diagnosis of intra-abdominal tumors, examination should be conducted following the administration of contrast medium. MRI is often superior to CT examination here, especially in connection with the extent of paravertebral tumors in the vertebral canal, as shown in the examples in figures 5 and 18 of tumors with intraspinal dissemination or origin in the vertebral canal.

For examinations in the abdomen, the use of special sequences for artifact suppression and an examination technique that accommodates the special needs of pediatric patients are recommended.

Musculoskeletal Examinations

MR imaging of the musculoskeletal system is less frequently performed in pediatric patients. X-ray is still the imaging method of choice for bone evaluation. Indications for MRI are better differentiation of bone defects diagnosed on radiographs (tumors, infections, benign cysts), secondary imaging when clinical findings cannot be explained by the radiographic finding, especially when the condition is caused by a soft tissue process, rheumatic disease and follow-up of musculoskeletal tumors. One of the important indications is the diagnosis and follow-up of osteomyelitis in pediatric patients as radiographs are often negative while MRI might reveal a skeletal edema consistent with the disease before any other imaging method becomes positive. In addition to the routine sequences with and without contrast enhancement, special fat suppressed sequences should therefore always be performed when evaluating the pediatric musculoskeletal system [figure 17].

Design-dependent Features Affecting Patient Monitoring and Sedation

The open design of the MAGNETOM Open system provides good visual and physical contact during the entire examination and thus facilitates patient monitoring; this is particularly advantageous when pharmaceutical sedatives are used. In our experience, the presence of the mother during the examination and the possibility of direct physical contact with her have a very positive effect on the cooperation of non-sedated children. Fig. 19 shows the process of a typical examination.

Special Technical Monitoring Features

We use a monitoring system from Bruker (Maglife) for technical monitoring of patients in our department; this system enables continuous measurement of transcutaneous pCO_2 and pO_2, capillary oxygen saturation, and terminal expiratory CO_2, as well as oscillatory and invasive arterial blood pressure measurement. The routine monitoring of sedated patients chiefly involves the measurement of capillary oxygen saturation and of the oscillatory blood pressure.

In our experience, the use of this monitoring system in its standard commercially available form results in considerable RF interference, with a significant deleterious effect on the quality of MR tomography images. This is the result of the increased sensitivity of open MRI systems to RF interference, which can reach the receiving coil more easily than it is the case for closed tubes with better shielding.

We have solved this problem by developing additional RF shielding for the monitoring system. This shielding is already available from the companies involved.

Overall, the ease of patient monitoring is significantly increased by the open system design: direct access to the patient is always available, and even malfunctions occurring during the examination process (for example, sensor dislocations) can easily be corrected without delay or interruption of the investigation.

Sedation of Uncooperative Children

In a retrospective and prospective study conducted in 1997-1998, we compared a cohort of children requiring sedation during use of our current system with data for 111 patients examined by us using a closed high-field MR system. Strikingly, we found that the sedation and anesthesia rate for our patients had decreased significantly, from 47 % to 27 % ($p < 0.001$), following introduction of the open magnetic resonance tomograph. This is principally the result of a considerably lower sedation rate for the age group up to 10 years (12).

Table 1 presents an overview of the sedation rate in a closed magnetic resonance system versus the sedation rate in an open system, broken down into 2 age groups. In the age group over 10 years, the decision for pharmaceutical sedation is determined by the patient's physical condition (for example, intensive care patients) or mental situation (statomotoric and mental retardation) rather than the design of the system and the examination process (13,14).

Examinations in high-field systems at our clinic were conducted exclusively using general anesthesia. In our experience, this can almost always be avoided in an open MRI, where sedation combining 0.2 mg/kg KG etomidate and 0.2 mg/kg body weight midazolam is sufficient for nearly all patients to ensure an uninterrupted examination. Although there have been no incidents during sedation in the last two and a half years, the presence of an investigator with experience in pediatric intensive medicine is necessary.

	Open Low-Field System *(Sedation)*	***Closed High-Field System*** *(General Anesthesia)*	***Significance Level***
Age ≤ 120 Months *examined/sedated*	*232/68 (29%)*	*84/51 (61%)*	*$p < 0.0001$*
Age > 120 Months *examined/sedated*	*42/6 (14%)*	*25/1 (4%)*	*n.s.*
Total *examined/sedated*	*274/74 (27%)*	*111/51 (47%)*	*$p < 0.001$*

Table 1:
Overview of sedation rates in a closed magnetic resonance system in comparison to an open magnetic resonance system, broken down into 2 age groups.

Interventions

Not only does the open system design allow for better contact with the patient in respect to monitoring, but it also enables intervention for diagnostic and therapeutic purposes. The open system design makes it easier to reach the target regions. Fast sequences can be used to track the needle in real time during a biopsy. These interventions can be performed with short-term pharmaceutical sedation.

In our center, for example, we performed a biopsie in a 7-year-old boy with status post treated oncological disease and current suspicion of a metastasis in a vertebral body. The conventional MRI of the spine had shown a destroyed thoracic vertebra. As an increased sensitivity to ionizing radiation was included in the differential diagnosis of this patient the puncture had to be undertaken under radiation free conditions. The biopsy was performed in a dorso-lateral position using MR monitoring. Necrotic tissue was confirmed histologically. The necrosis of the vertebral body was assumed to be a radiation side-effect resulting from the patient's increased sensitivity to radiation as further proven in the fibroblast cultures. Another patient who underwent an interventional biopsy presented with a cystic intra-abdominal lymphangioma. During the procedure a sclerosing agent (OK 432) was injected into the lymphangioma.

Overall, our experience shows that interventional procedures are easily performed in the open MR system. Methodological difficulties do arise, however, in the positioning of MR slice orientation for interventions; the use of markings on the body surface or needle probings at likely points of access can make this complicated. Further development of biopsy holders for automatic needle positioning would significantly increase the importance of MR-supported interventions by simplifying the necessary methods.

Prospects and Perspectives

While low-field MRI provides obvious advantages in the areas of sedation and patient access, this method's principal limitation lies in its inferior signal-to-noise ratio in comparison with high-field systems. If modern gradient echo sequences, for example, are used with considerably increased slice thicknesses to counteract this, the method will allow for MR images that are – in theoretical physical terms – qualitatively better than those obtained with high-field systems: some of the artifacts that occur with MRI increase with increasing field strength. With the use of very thick slices in the area of body diameter, projection volume images can be obtained that can be interpreted similar to conventional X-ray images in the area of the lung or the paranasal sinuses.

As an example, figure 20a shows the volume projection examination using thick slices in the area of the lung of a patient with cystic fibrosis. The follow up image [figure 20b] shows that acute changes are clearly noted and radiation free follow-up is possible. At a very short examination time (1.2-3.6 seconds), this examination method might be used in the future as an alternative to conventional X-ray examination of the thorax in pediatrics. This is currently being investigated in a prospective study conducted at our clinic (15). Due to the extremely fast imaging real-time MRI during respiration can also be performed easily. Another possible perspective is the fast imaging of the paranasal sinuses as presented in figure 21.

Conclusion

MRI is an important element in pediatric diagnostic imaging. Without using ionizing radiation, it provides outstanding imaging of anatomical relationships and tissue limits. In the low-field range, the open system design provides significant advantages such as a decrease in sedation rates, easier monitoring of sedated patients, and interventional diagnostics and therapy. At the same time, examination times are slightly lengthened and the signal-to-noise ratio is slightly inferior to those for high-field MR systems.

The future prospects for low-field MRI are new methods relying on modern gradient echo systems, which will enable fast imaging with a high signal-to-noise ratio. In some areas, these methods could come to supplant conventional X-ray exposures.

Literature

1. Fagan SJ, Byrd SE, Chuang HS, et al: Head and Spine Imaging; in Cohen MD and Edwards MK. (eds): Magnetic Resonance Imaging of Children. Philadelphia, BC Decker, Inc. 1990, pp 85-540.

2. Kangarloo H, Bach AM, Hilfer CL, et al. Chest MRI in children. Radiol Clin North Am 1998;8:1040-1046.

3. Klein MV, Hesselink JR: Brain: Indications, Techniques, and Atlas; in Edelmann RR, Hesselink JR and Zlatkin MB. (eds): Clinical Magnetic Resonance Imaging. Philadelphia, WB Saunders Company, 1996, pp 457-981.

4. Kuharik MA: Sedation, Anesthesia, and Patient Monitoring; in Cohen MD and Edwards MK. (eds): Magnetic Resonance Imaging of Children. Philadelphia, BC Decker, Inc, 1990, pp 75-84.

5. Link KM, Lesko NM: Congenital Heart Disease; in Edelmann RR, Hesselink JR and Zlatkin MB. (eds): Clinical Magnetic Resonance Imaging. Philadelphia, WB Saunders Company, 1996, pp 1683-1710.

6. Malmgren N, Hochbergs P, Holmqvist C, Sandström S, Laurin S, Björkhem G. Complex congenital heart malformation evaluated with MR imaging at 0.3 T. Pediatr Radiol 1996;26:470-477.

7. Mc Kenna W et al. Diagnosis of arrhythmogenic right ventricular dysplasia/ cardiomyopathia. British Heart Journal 1994;71:215-218.

8. Rupprecht T, König M, Nitz WR, Hofbeck M, Singer H, Böwing B. Möglichkeiten der Niederfeld NMR-Diagnostik bei kardiopulmonalen Erkrankungen im Kindesalter. Monatsschr Kinderheilkd 1997;145 (S1): S 155 (Abstract)

9. Rupprecht T, Böwing B, Rascher W, Kuth R, Deimling M. Steady State Free Precession Projektions NMR - Eine Alternative zu konventionellen Röntgenthorax Untersuchungen? Ergebnisse einer pädiatrischen Pilotstudie. Radiologe 1999;8:732-733. (Abstract)

10. Siegel MJ. Chest applications of magnetic resonance imaging in children. Top Magn Reson Imaging 1990;3:1-23.

11. Sieverding L, Jung W I, Fleiter T H, et al. Progress of MRI and variation of the diagnostic procedure in congenital and acquired heart disease. Klin Pädiatr 1992;204:340-347.

12. Rupprecht T, Kuth R, Böwing B, Gerling S, Wagner M, Rascher W. Sedation and Monitoring of Pediatric Patients undergoing Open Low Field MRI. Acta Paediatr 2000;89:1077-1081.

13. Carr JJ, Hatabu H, Gefter WB: Thorax; in Edelmann RR, Hesselink JR and Zlatkin MB. (eds): Clinical Magnetic Resonance Imaging. Philadelphia, WB Sunders Company, 1996, pp 1615-1682.

14. Cohen MD: Gastrointestinal System; in Cohen MD and Edwards MK. (eds): Magnetic Resonance Imaging of Children. Philadelphia, BC Decker, Inc. 1990, pp 611-678.

15. Volle E, Park W, Kaufmann HJ. MRI examination and monitoring of pediatric patients under sedation. Pediatr Radiol 1996;26:280-281.

T. Rupprecht, MD
University Pediatric Hospital
Loschgestrasse 15
D-91054 Erlangen
Germany

Exemplary Studies on Diffusion and Perfusion Weighted Magnetic Resonance Imaging in Acute Neurological Disease

A. Gass, J. G. Hirsch, S. Behrens, K. Szabo, J. Gaa, M. G. Hennerici
NMR Research Depts. of Neurology/Radiology, Universitaetsklinikum Mannheim, University of Heidelberg, Mannheim, Germany

Introduction

Magnetic resonance imaging (MRI) is increasingly used for the diagnosis and monitoring of neurological disorders, while established diagnostic methods show limitations in their ability to demonstrate the underlying pathophysiology and pathology. MRI frequently offers the "background" information needed for a rational basis for therapeutic decision making.

High resolution MRI using conventional contrasts (proton density-, T_2-, T_1-weighted, T_1-weighted after Gadolinium) can demonstrate with high sensitivity the site and extension of focal abnormality even in structures as small as the optic nerve or brain stem nuclei [1, 2]. Echo planar acquisition techniques have facilitated the use of perfusion weighted (PW) and diffusion-weighted (DW) magnetic resonance imaging (MRI) in a clinical setting [3, 4]. In addition to structural MRI they have the potential to visualize the earliest hemodynamic and tissue changes induced by ischemia and non-ischemic CNS pathologies. This is exemplified in serial MRI case studies of 4 patients with acute severe neurological deficits due to cerebral ischemia, focal epilepsy, acute relapse in multiple sclerosis (MS) and in suspected toxic/nutritional demyelination. All patients were investigated early after symptom onset and in follow-up studies with structural and echo planar diffusion and perfusion weighted MRI.

Materials and Methods

MRI data acquisition

MRI was performed on a 1.5 Tesla clinical scanner with EPI hardware (*VISION*, Siemens Medical Engineering Group, Erlangen).

1. Transverse, coronal, and sagittal localizing sequences followed by transverse oblique contiguous images (slice thickness 5 mm) aligned with the inferior borders of the corpus callosum (sequences 2.-5.).
2. Proton density (PD)- and T_2-weighted TSE (TR 2620 ms/ TE 14 ms/85 ms, FOV 180 x 240 mm², matrix size 192 x 256)
3. T_1-weighted SE (TR 530 ms/TE 12 ms, FOV 180 x 240 mm², matrix size 192 x 256)
4. DW SE-EPI (TR 4000 ms/TE 110 ms, b = 0/160/360/640/1000 s/mm², FOV 240 mm², matrix size 128 x 128, sequential application of 3 separate diffusion sensitising gradients in perpendicular directions).
5. Perfusion-weighted FID-EPI sequence following the first pass of a contrast bolus through the brain (TR 2000 ms/ TE 65 ms/Flip 90°, 13 slices, 40 acquisitions, 1:20 min, FOV 240 mm², matrix size 128 x 128). Contrast was injected manually through large gauge venous canula at the antecubital vein following a standardised protocol.

Data Processing and Analysis

DW MRI: ADC-maps were calculated on a pixel-by-pixel basis by a linear least-squares fit after averaging the direction-dependent DW images [3]. Manually defined regions-of-interest (ROI) were positioned in the regions of most pronounced signal change on DW images (b = 1000 s/mm²) and corresponding normal appearing tissue. These regions were superimposed on the calculated ADC maps.

PW MRI: From the data set a global time-intensity curve (a plot of the average signal as a function of time) was calculated for quality assurance of the bolus-passage (fig. 1). Two parameter maps, that evaluate qualitatively the main characteristics of the contrast bolus passage (i.e. the timing of arrival in the capillary bed and the amplitude of signal change) were calculated: A time-to-peak (TTP) map (i.e. the intensity of each pixel is related to the relative position of the peak of the bolus-passage curve), which shows the time of arrival of the contrast bolus in the parenchyma/veins and a signal change map (PBP – percentage of baseline at peak), that considers the amplitude of signal loss induced by the contrast bolus passage through the capillary bed.

Case Report 1

A 62 year old man presented 2 hours after acute onset of severe right sided weakness and speech disturbance. On clinical examination high grade right central hemiparesis and dysphasia were noted. Cerebral ischemia in the left middle cerebral artery (MCA) territory was suspected and emergency MRI was performed demonstrating a right MCA infarct in evolution. Intravenous rtPA therapy was initiated and on follow-up MRI reopening of the previously occluded MCA main stem and improvement of hypoperfusion in the MCA territory was observed. Doppler and duplex ultrasound studies revealed subtotal stenosis of the left internal carotid artery (ICA) and on day 3 carotid endarterectomy was successfully performed. Follow-up MRI demonstrated restoration of ICA flow signal and normalisation of MCA territory perfusion and the patient had a favorable outcome with only slight residual finger weakness.

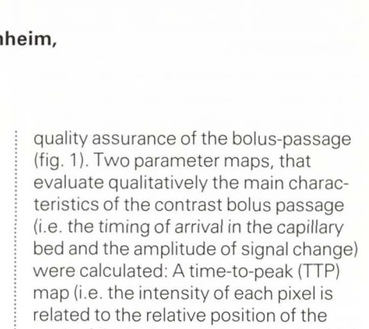

Figure 1
Plot of average signal as a function of time (global time-intensity curve), that is calculated for quality assurance of the bolus-passage.

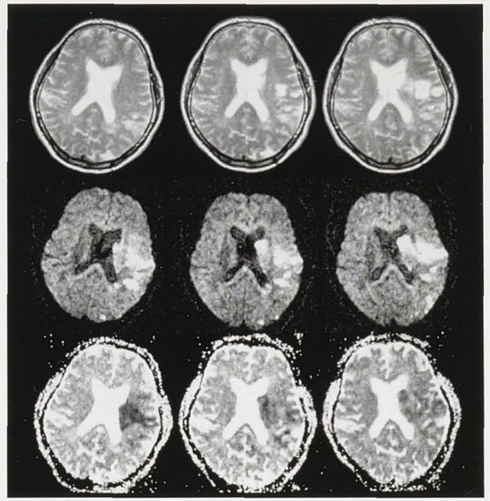

Figure 2a
Successful i.v. thombolytic therapy and subsequent carotid endarterectomy in acute stroke. MRI 2 hours after symptom onset (first column), 2 hours after i.v. thombolytic therapy (second column) and on day 3 after carotid endarterectomy is shown (third column). Initial T_2- and T_1-weighted images shows minimal abnormality, while diffusion weighted images and the ADC map reveal an early ischemic lesion in the left middle cerebral artery (MCA) territory. The area of hemodynamic compromise is considerably larger encompassing the whole MCA territory.

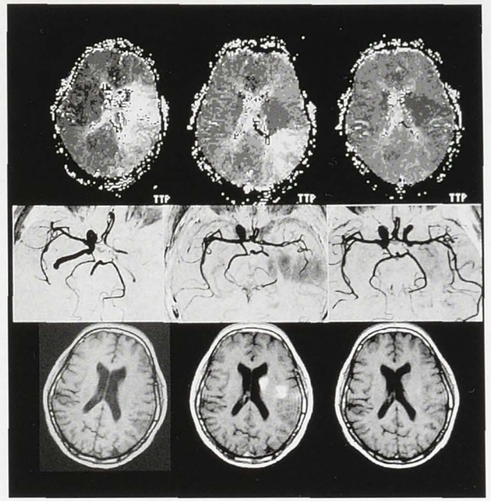

Figure 2b
On MRA no flow signal is detected in the left internal carotid artery (ICA) and MCA (second column, left). After i.v. thombolytic therapy flow signal is detected in the left MCA and the perfusion is normalized in the anterior part of the MCA territory (second column, middle and right). T_1-weighted shows transient hemorrhagic transformation of the ischemic lesion (third column). Subtotal ICA stenosis was diagnosed by Duplex ultrasound and carotid endarterectomy was performed. Postoperatively flow signal can be detected in the left ICA and MCA while perfusion shows complete normalization (first column). The area of infarction remained relatively limited compared to the initial risk of large MCA infarction.

Case Report 2

A 58-year-old patient was admitted to the emergency department 2 hours after sudden onset of left sided hemiparesis. The referring physician also reported "a nystagmus to the left and phases of altered consciousness". Previous history: Five months earlier angiographically confirmed cortical vein thrombosis had occurred and one month later symptomatic epilepsy was diagnosed after a first complex focal seizure and electroencephalographic confirmation of right centro-parietal rhythmic spike-slow-wave and sharp-slow wave activity.

On clinical presentation in the emergency room he had a hemianopic visual field defect to the left and a left sensory-motor paresis. Cranial CT examination detected no definite change compared to the previous scan 4 months earlier. MRI was performed 3.5 hours after symptom onset. At the end of the MRI examination clonic epileptic motor activity of the left leg occurred, that persisted when the patient was transferred from the scanner to his bed. Clonic activity stopped immediatedly after a dose of 7.5 mg diazepam. A diagnosis of Todd's paresis after suspected prolonged complex-focal ictal activity (probably for several hours) was made. MRI demonstrated a close spatial correlation of signs of regional hyperperfusion and a 22% reduction of the ADC in corresponding right parieto-occipital cortical tissue. Single-photon emission computed tomography (SPECT) confirmed focal hyperperfusion and EEG localized periodic lateralised epileptiform discharges in corresponding areas. Along with medical seizure control, perfusion and diffusion abnormalities were reversible.

Case Report 3

A 27-year-old woman with known relapsing-remitting MS was referred 1 day after onset of left sided weakness. On clinical examination there was severe pyramidal weakness of the right arm and leg. An acute relapse was suspected and conventional and DW MRI was performed. A new subcortical lesion involving pyramidal tract fibers on the right could be distinguished from

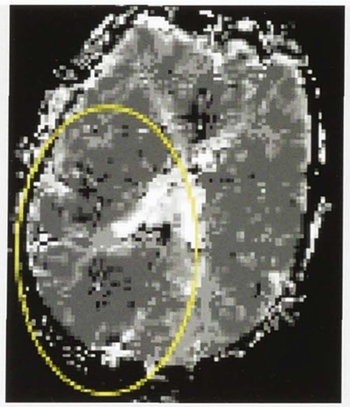

3a

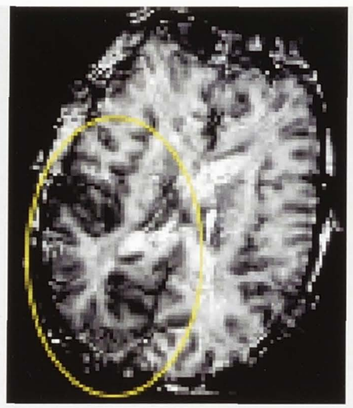

3b

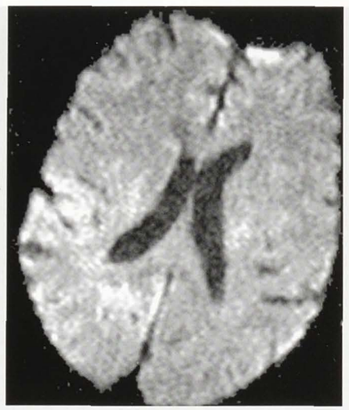

3c

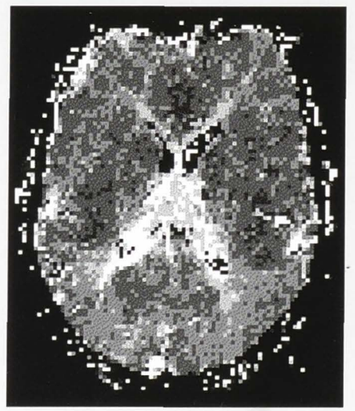

3d

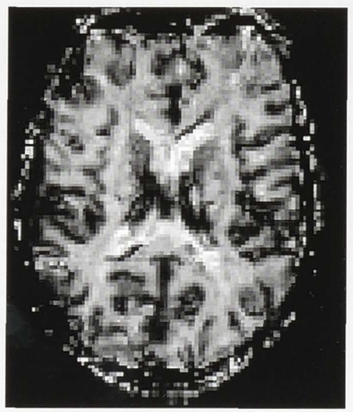

3e

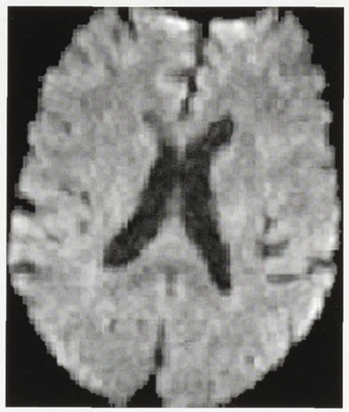

3f

Figure 3a-f
Ictal/postictal perfusion (left, center) and diffusion MRI (right) in the acute phase (top row) and follow-up (bottom row).

Signs of hyperperfusion are detected on PW MRI (TTP map left, PBP map center).

TTP and PBP maps show lower signal intensity indicating marked hyperperfusion in the right parieto-occipital region (encircled), accentuated in cortical regions. On the corresponding strongly DW image ($b = 1000\ s/mm^2$) hyperintensity can be seen in large parts of the right hemisphere (occipital and parietal lobes, parieto-occipital junction).

Hyperintensity is accentuated along the cortical band and in the paramedian occipital cortex.

The ADC was reduced by 22% (± 1%) compared to normal appearing ROIs in the contralateral hemisphere. Diffusion abnormalities have normalized on day 13 (bottom row).

Follow-up perfusion weighted MRI on day 3 shows resolution of perfusion changes with a normal, symmetric bolus passage on TTP and PBP maps.

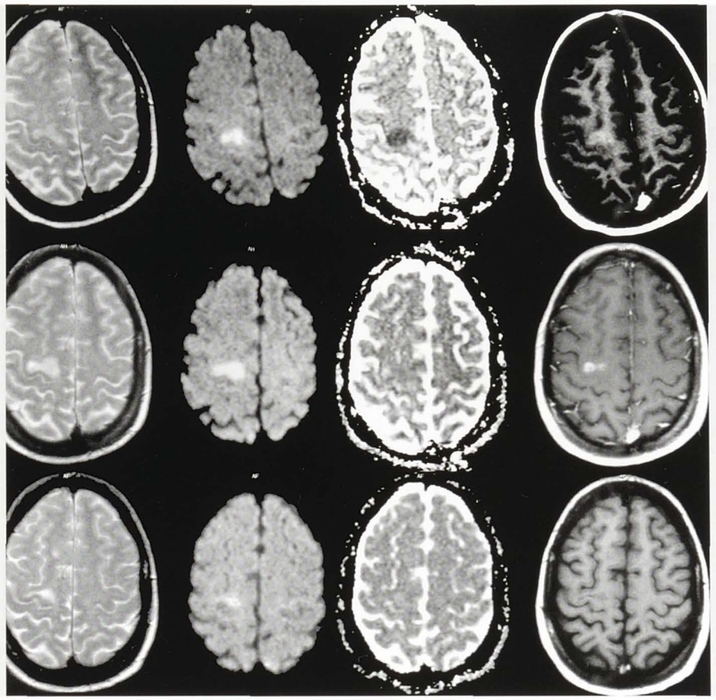

Figure 4
Serial MRI of an MS patient with an acute relapse and a new MS lesion.

T_2-, diffusion weighted, ADC, and contrast enhanced T_1-weighted MRI at presentation (top row), at day 5 (middle row), and at 4 weeks (bottom row):

At presentation the lesion shows slight T_2 hyperintensity, prominent ADC reduction, and minimal contrast enhancement on late post contrast images after appropriate windowing. At day 5, T_2 hyperintensity has increased while the ADC shows 'pseudo' normalization, and contrast enhancement shows up early and more prominently than before. At 5 weeks the lesion shows residual T_2 hyperintensity, slight ADC elevation, contrast enhancement has stopped.

chronic subcortical T_2 hyperintense lesions. This lesion showed initially a reduced ADC, minimal T_2 hyperintensity and only very faint contrast enhancement on late post contrast images (double dose Gadolinium-DTPA). High dose i. v. corticosteroid treatment was started for 3 days. On day 5 contrast enhancement and T_2 hyperintensity of the lesion were much stronger, while the ADC was "pseudo" normalized. The follow-up MRI at 5 weeks after the patient had made a nearly complete functional recovery showed a characteristic chronic constellation of a slight ADC elevation, T_2 hyperintensity and only slight T_1 hypointensity of the residual lesion.

Case Report 4

A previously healthy 29-year-old patient was referred from another institution with unexplained subacute onset of neurological symptoms. She had given birth to her first baby without any complications 6 weeks earlier. On the initial clinical examination she was fully oriented with psycho-motor slowing and slight dysarthria. Her motor function was impaired with abnormal choreatiform movements and her gait was markedly ataxic. On a cranial CT examination no definite abnormality was noted. EEG showed some generalized slowing but no focal abnormality. CSF examination was normal without any indication of CNS inflammation. Laboratory examinations were unremarkable.

Conventional and DW MRI was performed. Symmetrical white matter lesions with marked ADC reduction and T_2 hyperintensity were observed in a symmetrical distribution in the corpus callosum and in subcortical white matter in the centrum semiovale. There was no contrast enhancement and no evidence of any chronic lesions. A diagnosis of suspected toxic/nutritional demyelination was made. Over the following 8 weeks she made a continuous gradual improvement with a favorable outcome with some residual dysarthria and slight gait abnormalities.

Discussion

In these case studies of patients presenting with acute neurological deficits, lesions with a reduced ADC are described in 4 different disorders: cerebral ischemia, after a prolonged complex-partial seizure, in the early stage of the development of an inflammatory-demyelinating lesion and in suspected toxic/nutritional demyelination. In all cases the location and the extent of the acute abnormality were identified, which correlated well with the clinical features at presentation. PW MRI clearly separated the typical pattern of hypoperfusion in cerebral ischemia from the state of hyperperfusion as a sequel of increased glucose utilisation due to prolonged epileptic activity. In acute stroke, MRI identified not only the vasular pathology, the area of hypoperfusion und a reduced apparent diffusion coefficient (ADC) in the infarct core, but visualized successful recanalisation therapy (i.v. thombolytic therapy and carotid end-arterectomy) in follow-up studies.

Reduction of the ADC delineated an acute phase of disease which was followed by elevated or normalized ADC values in chronic stages. This pattern is well recognized in stroke but is much more rarely seen in postictal MRI and in acute MS lesions [5-7]. In patients 1-3 chronic lesions (with T_2 hyperintensity and elevated ADCs) were easily differen-

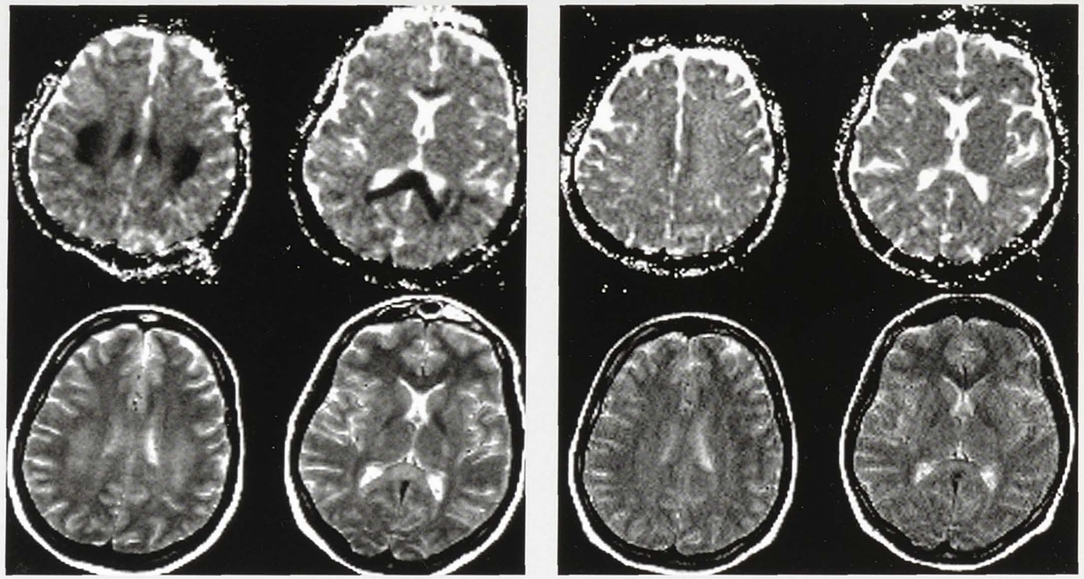

Figure 5
T_2- and diffusion weighted follow-up MRI in suspected toxic demyelination.

Left box – at presentation. Right box – follow-up at 4 weeks:

Left: Extensive white matter lesions with ADC reductions (top row) are noted in the genu and splenium of the corpus callosum and in the subcortical white matter in a symmetrical distribution. On T_2-weighted images corresponding hyperintense lesions are seen except for the lesion in the genu of the corpus callosum that appears isointense to normal white matter.

Right: At 4 weeks the ADC has normalised and no obvious residual T_2 abnormality or tissue atrophy has developed.

tiated from the acute pathology indicated by the ADC reduction in symptomatic lesions. Chronic lesions in stroke and MS usually show signs (T_2 hyperintensity, T_1 hypointensity, ADC elevation) of persistent tissue destruction (due to necrosis, demyelination, axonal loss) [8]. In patients 3 and 4 (after epileptic activity, after suspected toxic/nutritional demyelination) there were no unequivocable signs of tissue destruction on follow-up ADC maps or T_2-weighted images. This indicates that low ADCs in acute human white matter lesions occuring in the context of different pathophysiological mechanisms do not share the same prognosis.

The location of all lesions with an ADC reduction correlated with severe neurological deficits. The relationship of functional neurological status and ADC reduction has rarely been addressed in animal experiments. ADC reductions of about 25 % as in the patient with prolonged ictal activity may be sufficient to compromise neuronal/axonal electrical capabilities [9]. Correlations of clinical status and lesion volumes have been repeatedly reported in acute stroke, when a more pronounced ADC decrease is usually found (40-50 %) [4, 10]. Further studies into the relationship of the ADC and functional status are needed to substantiate how closely ADC reductions correlate with neuronal/axonal dysfunction.

There is no definite explanation why different pathophysiologies may lead to a reduced ADC. Experimental work in ischemia and epilepsy suggests, that compromised energy metabolism and a rise of lactate induce ADC reductions [9, 11]. Prolonged ictal activity is known to increase glucose utilization, the increase of which is not adequately matched by the enhanced blood flow (12, 13). As a result, blood flow-metabolism uncoupling leads to a reduction of high-energy adenosine phosphates and tissue hypoxia, thereby stimulating anaerobic glycolysis (14). In experimental inflammatory white matter lesions it has been suspected that toxic inflammatory changes (cytokines, oxidative products, proteolytic enzymes) in active lesions may cause mitochondrial dysfunction and lead to metabolic compromise inducing a reduction of the ADC [15,16].

PW and DW MRI can provide complementary information to high resolution structural MRI providing new insights into the pathophysiology of acute neurological diseases. This offers new approaches for research as well as valueable diagnostic information in clinical practice.

Literature

[1] Gass, A., Filippi, M., Grossman, R. I.:
The contribution of MRI in the differential diagnosis of posterior fossa damage.
J Neurol Sci 2000; 172 Suppl 1:43-S49.

[2] Gass, A., Moseley, I. F.:
The contribution of magnetic resonance imaging in the differential diagnosis of optic nerve damage.
J Neurol Sci 2000;172 Suppl 1:17-S22.

[3] Le Bihan, D., Breton, E., Lallemand, D. et al.:
MR Imaging of Intravoxel Incoherent Motions: Application to Diffusion and Perfusion in Neurologic Disorders.
Radiology 1986;161:401-407.

[4] Warach, S., Dashe, J. F., Edelman, R. R.:
Clinical outcome in ischemic stroke predicted by early diffusion-weighted and perfusion magnetic resonance imaging: a preliminary analysis.
J Cereb Blood Flow Metab 1996; 16(1):53-59.

[5] Warach, S., Gaa, J., Siewert, B., et al.:
Acute Human Stroke Studied by Whole Brain Echo Planar Diffusion-weighted MRI.
Ann Neurol 1995; 37: 231-241.

[6] Wieshmann, U. C., Symms, M. R., Shorvon, S. D.:
Diffusion changes in status epilepticus.
Lancet 1997;350(9076):493-494.

[7] Tievsky, A. L., Ptak, T., Wu, O., Farkas, J., Gonzalez, R. G., Rosen, B. R., Sorensen, A. G.:
Evaluation of MS lesions with full tensor diffusion weighted imaging and anisotrópy mapping.
ISMRM 1997:666-666.

[8] Horsefield, M., Larsson, H., Gass, A.:
Diffusion weighted Magnetic resonance imaging in multiple sclerosis.
J Neurol Neurosurg Psych suppl 1997; 64(suppl):80-S84.

[9] Zhong, J., Petroff, O. A. C., Pleban, L. A., Prichard, J. W., Gore, J. C.:
Reversible, reproducible reduction of brain water apparent diffusion coefficient by cortical electroshocks.
Magn Reson Med 1997;37(1):1-6.

[10] Lovblad, K.O., Baird, A.E., Schlaug, G., et al.:
Ischemic lesion volumes in acute stroke by diffusion-weighted magnetic resonance imaging correlate with clinical outcome.
Ann Neurol 1997;42(2):164-170.

[11] Gyngell, M., Back, T., Hoehn-Berlage, M., Kohno, K., Hossmann, K.-A.:
Transient cell depolarization after permanent middle cerebral artery occlusion: An observation by diffusion-weighted MRI and localized 1H-MRS.
Magn Reson Med 1994;31:337-341.

[12] Hoshi, Y., Tamura, M.:
Cerebral oxygenation state in chemically-induced seizures in the rat – study by near infrared spectrophotometry.
Adv Exp Med Biol 1992;316:137-42.

[13] Blennow, G., Nilsson, B., Siesjo, B. K.:
Influence of reduced oxygen availability on cerebral metabolic changes during bicuculline-induced seizures in rats.
J Cereb Blood Flow Metab 1985; 5(3):439-45.

[14] Blennow, G., Folbergrova, J., Nilsson, B., Siesjo, B. K.:
Cerebral metabolic and circulatory changes in the rat during sustained seizures induced by DL-homocysteine.
Brain Res 1979;179(1):129-46.

[15] Heales, S. J., Bolanos, J. P., Stewart, V. C., Brookes, P. S., Land, J. M., Clark, J. B.:
Nitric oxide, mitochondria and neurological disease.
Biochim Biophys Acta 1999 Feb 9; 1410(2):215-28.

[16] Blamire, A. M., Anthony, D. C., Rajagopalan, B., Sibson, N. R., Perry, V. H., Styles, P.:
Cytokine Induced Inflammation Causes Alterations in Brain Water Diffusion and Cerebral Perfusion. Proc. Intl. Sot. Mag. Reson. Med. 8 (2000) 485.

Author's address

PD Dr. A. Gass
NMR Research Neurology/Radiology
Universitätsklinikum Mannheim
Universität Heidelberg
Theodor-Kutzer-Ufer

D-68137 Mannheim, Germany
Tel: +49-6 21-3 83-28 85
Fax: +49-6 21-3 83-38 07
e-mail: gass@neuro.ma.uni-heidelberg.de

:Advancements in MRI Scanner Technology Lead to Improved Functional Imaging:

A. G. Sorensen
MGH-NMR Center, Massachusetts General Hospital, Charlestown, USA

Introduction

MRI has generally excelled at depicting anatomic changes in the brain. Over the past decade, however, MRI has increasingly been used to image physiologic changes in the brain, including changes associated with brain function and dysfunction. Responding to the demand for physiologic imaging, equipment capabilities are beginning to be expanded; this in turn is allowing improvements in physiologic brain imaging to begin to reach clinical practice. This article will review a few of the basic technical advances that suggest near term and long term clinical applications. Clinical image examples shown in this article have been acquired on a Siemens 1.5T MAGNETOM Sonata and a 3T MAGNETOM Allegra system.

The Need for More SNR

Perhaps as much or more than any other MRI technique, physiologic imaging is limited by the signal to noise ratio (SNR). Broadly defined, physiologic imaging, also termed functional imaging includes diffusion-weighted imaging (DWI); perfusion-weighted imaging (PWI), including techniques with and without exogenous contrast agents; brain activation imaging using blood oxygen level-dependent (BOLD) and blood flow techniques; and various other experimental techniques. Physiological imaging also includes spectroscopic imaging; although issues surrounding spectroscopic techniques warrant a separate discussion than will be undertaken here, to first approximation many of the same technical requirements imposed by the already mentioned advanced techniques are also needed by spectroscopic imaging. Conversely, spectroscopic imaging stands to benefit from the hardware and software advances that have been recently made just as other types of physiological imaging do.

MR Signal Increases with Field Strength

Investigators have used numerous approaches to try to overcome these SNR limitations. Many of these techniques such as acquiring multiple signal averages, use of surface coils, and sequence optimization often still leave physiologic imaging limited by SNR. As a result, additional approaches are being utilized. One approach is to move to higher field strengths. Work at a number of institutions has confirmed that higher field strength does indeed provide improvements in SNR and thereby in imaging performance for physiological imaging. Fig. 1 shows an example of this for BOLD imaging in a cognitive paradigm. Because BOLD imaging detects only a small change in signal compared to background fluctuations, the improvement in SNR translates effectively into a reduction in background fluctuations and therefore improved statistical confidence regarding what changes represent signal and what changes represent noise. This improvement in raw SNR by moving to higher field will benefit most if not all forms of functional imaging. Many investigators believe that such improved SNR will be essential if functional imaging is to meet its full clinical potential.

Overcoming High Field Artifacts

Some investigators have felt that moving to higher field strength such as 3T might come at too great a cost. In particular, since the susceptibility sensitivity also increases roughly linearly with field strength, there has been some concern that in areas near the base of the skull or in the posterior fossa there would be artifacts that would preclude gaining useful information from the brain in these areas. However, this does not appear to be necessarily the case. We have found that by moving to thinner slices (something that one wishes to do typically with increased SNR anyway), the intravoxel dephasing and incoherence is decreased (as a result of the smaller voxel size) and in fact susceptibility effects can decrease. An example of this is shown in fig. 2, where single shot echo-planar imaging is obtained throughout the brain including the cerebellum and brain stem and down in to the superior cervical spine without image degradation.

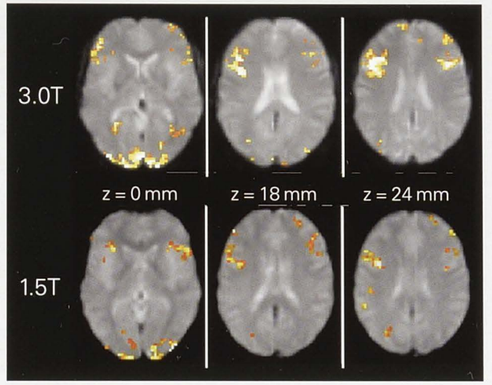

Figure 1
3T versus 1.5T activation. Comparison of activation in a group of subjects performing a word-generation task to visual stimuli at 3.0T (top row) and at 1.5T (bottom row).

Note the more extensive and stronger (as evidenced by the higher intensity color) activation in all regions. Note that additional noise is not produced, but rather additional signal consonant with the type of paradigm used.

Courtesy of Russell Poldrack, PhD.

Figure 2
Coverage at 3.0T of brain, cerebellum/ brainstem, and superior cervical spine.

Note the lack of warping, signal dropout, or other overt signs of susceptibility effects.

Technical parameters:
Gradient Echo EPI, 3.0T, TR 3000 ms, TE 50 ms, 3 mm slice thickness, no gap, single shot interleaved acquisition, 48 slices.

Courtesy of Larry Wald, PhD.

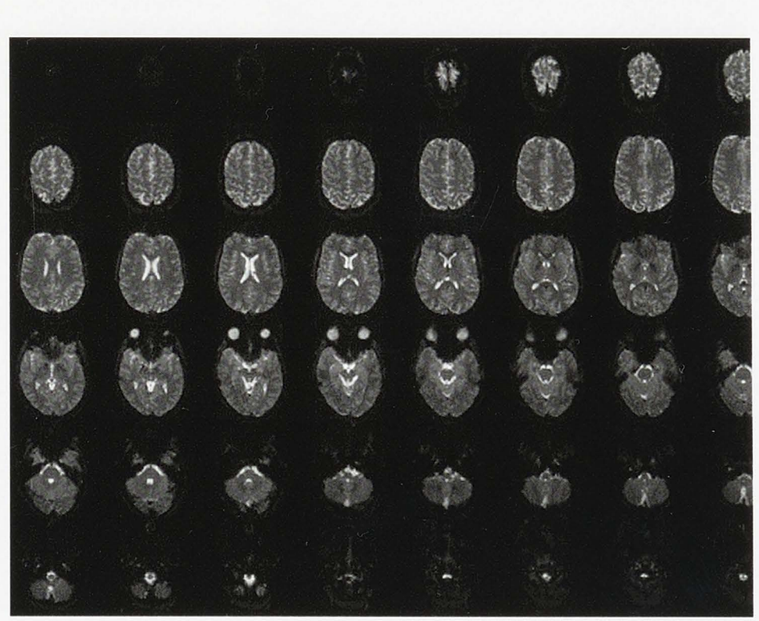

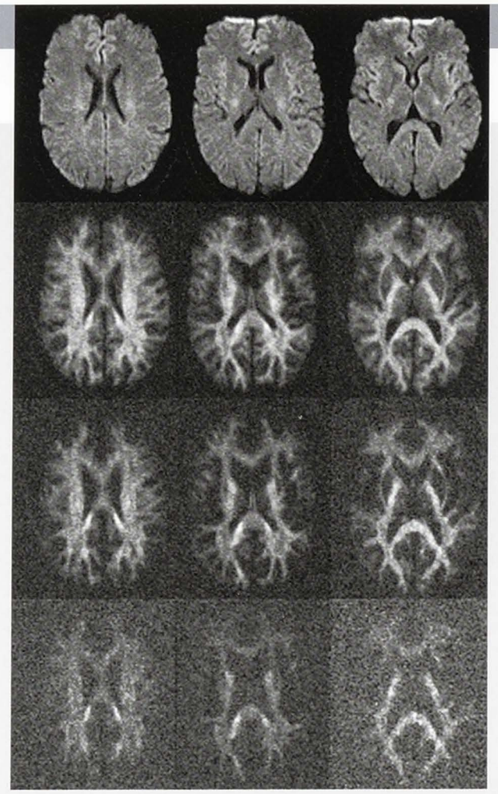

Figure 3
Very high b value diffusion weighted imaging. All images are trace-weighted from full tensor acquisitions at 1.5T with a 40 mT/m system. Images through the brain in this normal volunteer demonstrate routine appearance at b = 1,000 s/mm² (top row, 3 signal averages).

Note that at b = 5,000 s/mm², there is now marked gray-white contrast present whereas at 1,000 s/mm² there is little contrast (and what contrast is present at b = 1,000 is based mainly on T_2 differences). However, at b = 5,000 s/mm² (second row, 12 signal averages) there are clearly new phenomena occurring including apparently different rates of water diffusion in gray versus white matter, as well as a drop in signal to noise ratio due to the very high b value used.

This trend continues at b = 10,000 s/mm² (third row, 20 signal averages), where there are still increased gray-white differences compared to b = 1,000 s/mm², until at b = 20,000 s/mm² the gray matter is essentially invisible. This is probably due to non-monoexponential decay in the brain, but this is a matter of ongoing research.

Note that even for b = 20,000 s/mm² on a 40 mT/m system with all three axes able to operate simultaneously the TE is 136 ms (as compared to 67 ms for b = 1,000 s/mm²). This makes the visualization of white matter possible at b = 20,000 s/mm2 with 20 signal averages; if less SNR were available (if, for example, the TE was substantially longer), many more signal averages would be needed since SNR goes as the square root of the number of signal averages.

Note that the system is capable of 40 mT/m in all three gradient directions simultaneously, for a net performance of (square root of 3 times 40 mT/m) approximately 69 mT/m.

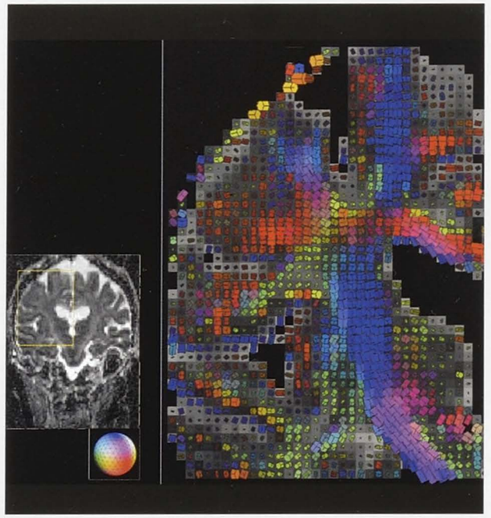

Figure 4
Diffusion tensor tractography of the in vivo human brain.*

This tractography study is from a 68 year old female with motor weakness but no evidence on any imaging study (including this tractography study) of any physical defect.

The multicolor area is an enlarge-ment of a coronal section through the brain.

The eigenvalues and eigen-vectors were then computed, weighted by the fractional anisotropy in the image, and overlaid on to an anatomic scan.

Note the clear directionality of the fiber bundles including the corpus callosum, cortico-spinal tracts, and subcortical U fibers.

Data were obtained on a 1.5 T system with 40 mT/m gradients and 18 signal averages of a single tensor acquisition sequence.

Courtesy of Mette Wiegell, David Tuch, and Van Wedeen MD.

Balanced System Architecture

Other approaches to improving SNR can be as important and as helpful as the increase in field strength. Indeed, the entire MRI system must be engineered to optimize SNR at each step: the magnetic field, the gradient subsystem, the RF chain, and the computer systems to handle both control of the system and the acquisition and processing of the data that are obtained. For example, it is well known that surface coils can improve SNR in a local area just underneath or near the surface coil. Numerous groups have demonstrated that one approach to improving SNR over a larger area than just a surface coil is to create arrays of surface coils. However, for functional imaging, an array-aware system is not enough. The RF receivers and digitizing hardware must be able to handle the high throughput of data on each of the multiple channels, rather than just on a single channel if phased array functional imaging is to actually be usable. This means four, eight, or more fast receivers, something that needs to be deliberately engineered in to the MR system. Similar issues arise with the computational chain: there is no point in having fast RF and gradient hardware to sample the magnetization rapidly if the computing subsystem cannot store or process the incoming data.

Gradient System Performance

A key subsystem that has been a focus of improvement recently is the gradient subsystem. While slew rates on the order of 100 T/m/s were once considered to be high, such systems are now underpowered for the rapid read-out pulse sequences in use today. Similarly, while peak gradient strength of 20 mT/m was only recently considered high performance, many users find their needs for peak gradient strength to keep increasing well beyond the 40 mT/m routinely offered today. This need for high peak gradient performance is particularly true in diffusion-weighted MR imaging. Fig. 3 demonstrates images from a normal volunteer taken at multiple high b values, including up to b = 20,000 s/mm². (Normal DWI is obtained at b = 1,000 s/mm²). Such very high b value images are highly dependent on adequate SNR, since the large diffusion gradients cause extensive signal loss. By increasing peak gradient strength, one can shorten the duration of the gradient pulses and markedly reduce the overall echo time of a given pulse sequence. Because diffusion-weighted images typically have long TE values (due to the long diffusion gradient pulse length), decreasing the TE from 100 ms (typical with gradient capabilities of approximately 20 mT/m) to TE of 65 ms (typical with gradient capabilities of 40 mT/m) one can expect a doubling of SNR. Particularly because very high b values are highly dependent on peak gradient strength and amplifier duty cycle, engineering the system from the ground up to handle such advanced performance requirements is essential.

Towards New Frontiers in Neuroscience

Once these systems are in place, however, the type and quality of functional imaging that can be done is dramatically increased. To close with just a single example, Fig. 4 demonstrates diffusion tensor tractography* performed using 40 mT/m gradients at 1.5 T in the brain. The type of tractography and the resolution available are highly dependent on the shortened TE, the faster gradient and RF performance, the amplifier capabilites, and the computer control and data processing subsystems. With the advent of this type of functional imaging, diagnoses of more subtle abnormalities and insight into more complex disease processes will be available in ways that were heretofore unavailable.

Author's address

A. Gregory Sorensen, MD
MGH-NMR Center
Massachusetts General Hospital
Building 149, 13th Street
Charlestown, MA 02129
USA

** This information about diffusion tensor tractography is preliminary. The product is under development and not commercially available in the U.S., and its future availability cannot be ensured.*

Software upgrade Numaris 3B33F for MAGNETOM Open/Open Viva/Open Viva #P

The literal meaning of "Viva" is "Live a long life". The word "Viva" is used to express Goodwill and Approval. The Numaris 3B33F software is precisely achieving this objective. Numaris 3B33F for the MAGNETOM Open/Open Viva/ Open Viva #P is further enhancing the capabilities of the system. Most of the sequences (.vhc) exploit the 15 mT/m gradient strength. MAGNETOM Open can do the routine "Bread and Butter" examinations with excellent Image quality.

Overview

The 3B33F software has the following new sequences:

- **Sequence with low TR and low TE (8 ms)**
  - → for better T_1 contrast
  - → for increased anatomical coverage as more slices per TR are possible
  - → for use in C-Spine and orthopedic imaging as well
- **Sequences for MR Cholangiography**
  - → for non invasive study of the biliopancreatic ductal system
  - → for imaging the extraductal structures as well
  - → with thick slab and thin slice (HASTE) techniques
- **LOTA Sequences**
  - → for reducing respiratory and motion artifacts
  - → for abdomen, C-Spine imaging
- **Single Shot U-FLARE sequence for Diffusion Imaging**
  - → for diffusion imaging in a few seconds (9 sec)
  - → with a b value of 600 sec/mm^2
  - → for advanced neuro applications
- **In Phase/Opposed Phase Sequence for Body Imaging**
  - → for liver diseases
  - → for pancreatic imaging
  - → for adrenal abnormalities
- **Sequences for Musculoskeletal Imaging**
  - → for better resolution knee, shoulder and other joints
  - → small FOV (130 mm) DESS, FLASH and FISP sequences
  - → 3D water excited sequences for pre and post contrast T_1 weighted images with fat suppression
- **2D True FISP Sequences for Lung Imaging***
  - → for very fast T_1/T_2 contrast of the lung with or without breathhold

* *Cardio Option*

Spin Echo sequence with low TR and low TE (8 ms)

The sequence se_8b130.vhc provides a short TE of 8 ms for better T_1 contrast. The short TE reduces the flow artifacts from the carotids. There are 19 slices available within a TR of 395 ms. This maintains the T_1 contrast and has a good anatomical coverage. The results are better than the sequence with TE of 15 ms, which was previously available. This sequence is also useful for T_1 C-Spine imaging as well as in joint imaging.

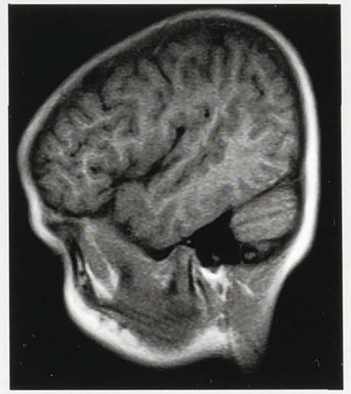

Spin Echo, 5:31 min, 5 mm, FOV 230 mm, 168 x 256 matrix

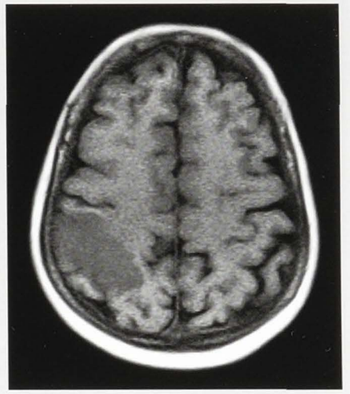

Spin Echo, 4:57 min, 5 mm, FOV 230 mm, 144 x 256 matrix

Sequences for MR Cholangiography – MRCP

The sequences for MRCP are the single shot TSE slab and HASTE thin slice technique. Similar to the sequences on the high field systems these sequences allow non-invasive breath-hold studies of the biliopancreatic system in few seconds. MRI has the added advantage of imaging the extra-ductal structures. Transverse T_1 and T_2 weighted imaging using LOTA provides additional information.

Courtesy Bhavin Jankharia M.D., JIC Mumbai, India

Case of Cholangiocarcinoma

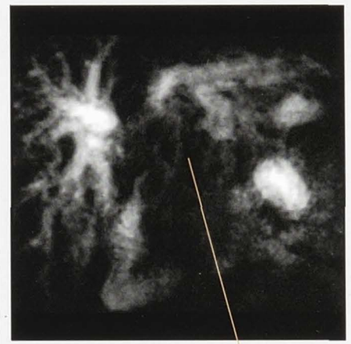

Thick Slab MRCP aquired in 2.89 seconds

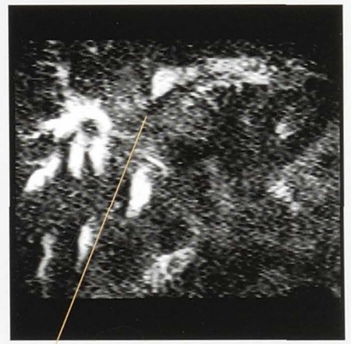

Thin Slice HASTE aquired in 15 seconds

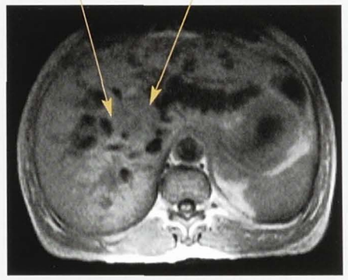

T_1 LOTA tra, 4:31 min

LOTA Sequences

LOng Term Averaging is a technique that reduces respiratory and motion artifacts. This technique is best used in body imaging. LOTA sequences can be used for good C-Spine imaging as well. T_1 and T_2 LOTA sequences are available with the Numaris 3B33F software.

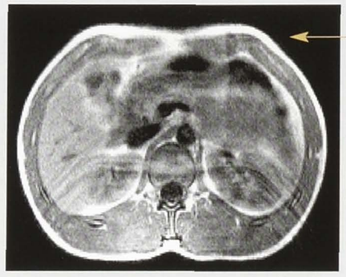

Standard averaging

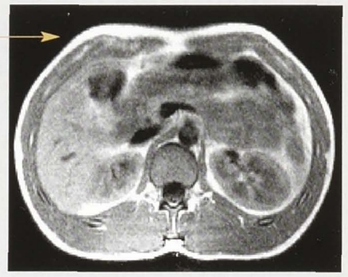

LOTA averaging

Single Shot U-FLARE sequence for Diffusion Imaging

A few years ago diffusion imaging on the low field was a difficult hypothesis in itself. With the Single shot U-FLARE sequence Siemens has achieved diffusion weighted imaging on the MAGNETOM Open, using all 3 diffusion sensitizing gradients simultaneously. U-FLARE takes only 9 seconds!!!! The following clinical examples demonstrate the S/N and excellent image quality.

The U-FLARE sequence is a single shot Turbo Spin Echo variant. In its simplest form it has 10 single shots averaged requiring 0.5 seconds/image with a matrix of 128 x 128. The scan has two sets of images, one with a "b" value of 0 sec/mm² called T_2 reference image and a second set of images with a b value of 600 sec/mm².

Courtesy Bhavin Jankharia M.D., JIC Mumbai, India

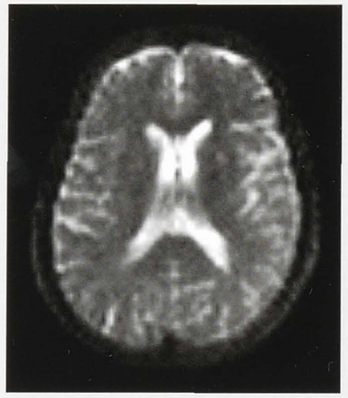

T_2 weighted reference image
b ≈ 0 sec/mm²
TE = 102 ms

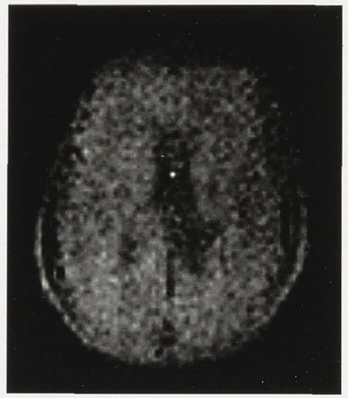

Diffusion weighted image
b ≈ 600 sec/mm²
TE = 102 ms

Example of a 60-year-old female with right MCA infarct

Courtesy Bhavin Jankharia M.D., JIC Mumbai, India

Spin Echo T_1, 4:57 min

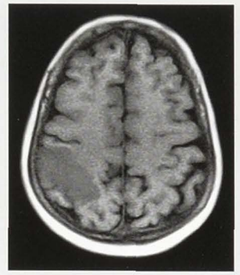

Turbo SE T_2, 4:59 min

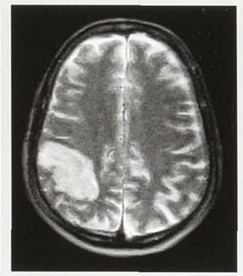

Dark Fluid T_2, 5:16 min

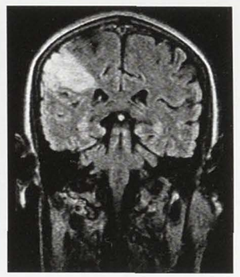

T_2 weighted reference image, b ≈ 0 sec/mm²

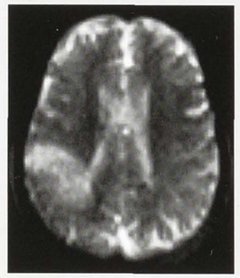

Diffusion weighted image, b ≈ 600 sec/mm²

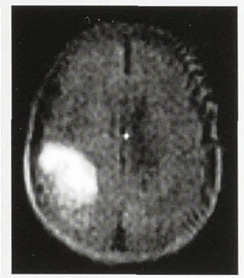

Example of a 40-year-old male with venous infarct

Courtesy Bhavin Jankharia M.D., JIC Mumbai, India

T_1 sagittal

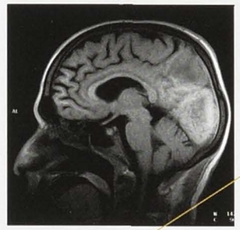

MR Venogram

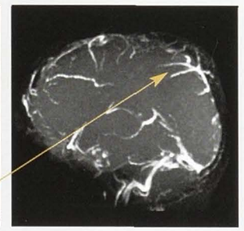

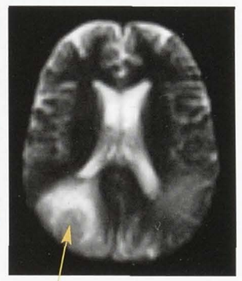

T_2 weighted reference image, b ≈ 0 sec/mm²

Multiple collateral venous channels due to thrombosis of sagittal sinus

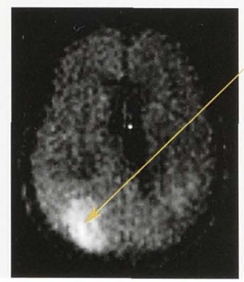

Diffusion weighted image, b ≈ 600 sec/mm²

Note:
The hyperintense signal on DWI is represented by hypointense signal on the T_2 reference image – an area of decreased diffusion.

In Phase – Opposed Phase Sequence for Body Imaging

At a particular TE (TE = 5.4 ms), when fat and water are in phase both signals add within a voxel, while at another TE (TE = 18.1 ms), fat and water protons are out of phase and their signals cancel each other in the same voxel. In the double echo sequence, 2 sets of images are acquired (in the same sequence) with two different TEs. In the images with opposed phase, hypointense regions contain fatty components. This is particularly useful in adrenal imaging. Secondly, the viscera get a sharper edge, differentiating the structures better. In the example below besides the viscera having a sharper edge, the signal from the bone marrow changes significantly. The Out of phase image has a better S/N as its bandwidth is narrower than the in phase image with very short echo time. Low bandwidth sequences improve S/N – *a definite advantage on Low field!*

In phase image (TE = 5.4 ms)

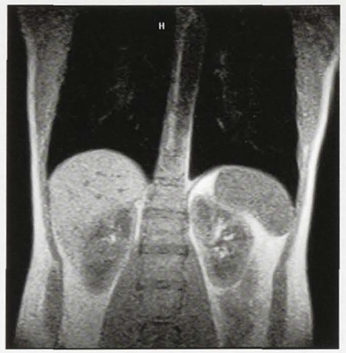

Out of phase image (TE = 18.1 ms)

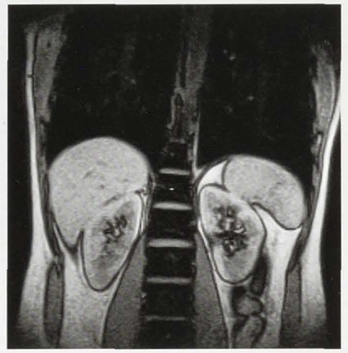

Sequences for Musculoskeletal Imaging

DESS, FLASH and FISP 3D sequences permit small FOV (130 mm) imaging for higher resolution. This will further enhance joint imaging on MAGNETOM Open. The two dimensional table movement enables isocentre positioning of the joint, like the shoulder yielding optimum image quality. The 3D water excited sequence is useful for pre- and post-contrast T_1 weighted joint imaging with fat suppression. Accurate frequency for water excitation has to be determined before the scan for good results.

Left: Courtesy Bhavin Jankharia M.D., JIC Mumbai, India
Right: Courtesy MRI ofEaston, USA

DESS 3D, 2 mm, 130 mm FOV

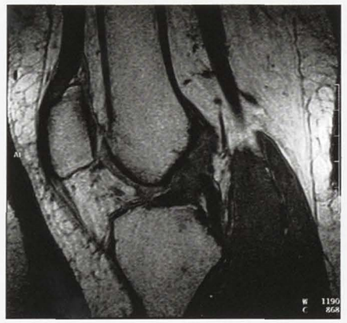

Water excitation, 3D, 3 mm, 220 FOV

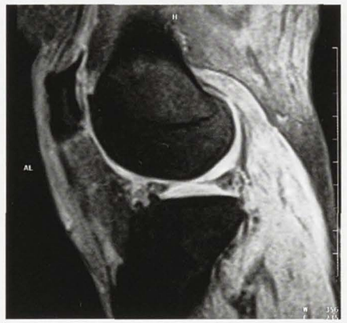

2D True FISP for LUNG Imaging*

Siemens is currently the only vendor offering True FISP, especially on low field. The 2D True FISP sequence is a very fast (subsecond to a few seconds) sequence. It is well suited for imaging lung parenchyma without contrast. Initial studies have shown that it is a promising alternative to conventional chest x-ray in pulmonary disease particularly in the pediatric age group where repeated x-ray should be avoided. A low magnetic field is an advantage in using this procedure.

X-ray

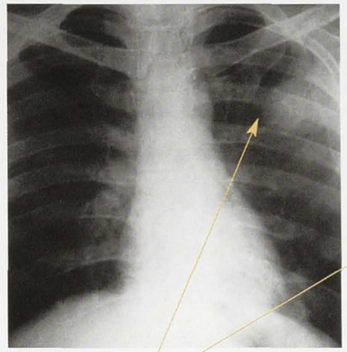

2D True FISP in 3 sec, 256 matrix

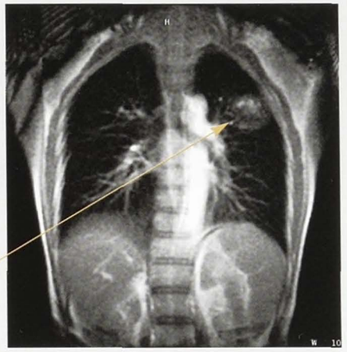

Courtesy Bhavin Jankharia M.D., JIC Mumbai, India

Pulmonary Vasculature
Case of Pneumonia – logarithmic scale

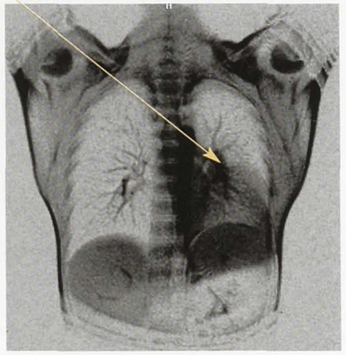

Courtesy: Dr.Th.Rupprecht et.al., Kinderklinik Uni-Erlangen, Germany

** Cardio Option*

:CP Body Array Flex Coil and CP Body Array Extender for MAGNETOM Harmony/Symphony/Sonata:

CP Body Array Flex and CP Body Array Extender are suitable for all high resolution body examinations such as thorax, abdomen, pelvis, etc. Each coil contains 2 CP elements for optimal SNR. The flexible design creates high patient comfort and ease of use. The coils are used in combination with the CP Spine Array Coil. They can easily be used together providing large field-of-view coverage to acquire for example thorax-liver or whole body MR angiography studies. Combining the coil element from within the user interface allows large anatomical coverage or targeted high resolution without the need of repositioning the patient or the coil by using remote table control.

CP Body Flex Array/ Peripheral CP Angio Array for peripheral MRA

CP Body Array Flex can be combined with Peripheral CP Angio Array Coil to perform high-resolution peripheral angiography including the lower abdominal aorta and iliac arteries.

Clinical result

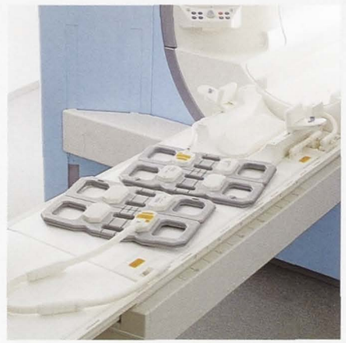

Fig. 1

Technical data for both coils:

4 coil design with 4 integrated preamplifiers

Integrated preamplifiers increases the signal-to-noise ratio and eliminates degradation of the signal during transfer

CP design offers up to 40% higher signal-to-noise than linear design

Array technology allows the coverage of large fields-of-view for high quality abdominal imaging

IPA™ coil concept allows intelligent combination of coil elements from different coils providing easy access to all anatomical areas

No-tune coil
(no patient-dependent tuning is necessary)

Size: 316 mm x 460 mm x 36 mm

Weight: only 1.1 kg !

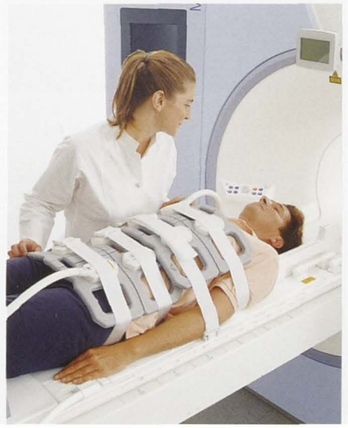

Fig. 2

Coils positioned on patient for large FoV imaging. Remote "Table motion" allows the region of examination (pelvis) to be placed in the center of the magnet. "Integrated panoramic positioning with automatic coil element switch" chooses the coil at iso-center automatically from upper elements to lower elements

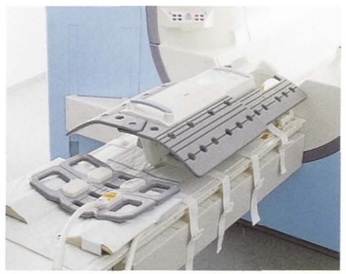

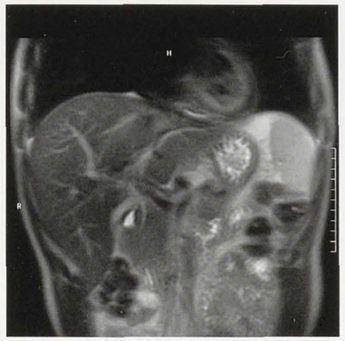

Fig. 3
liver coronal

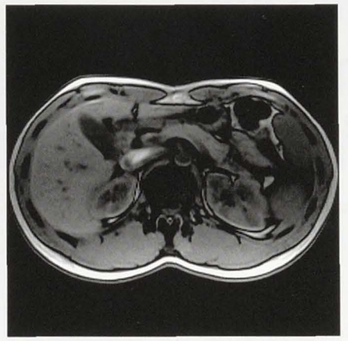

Fig. 4
FLASH in-out phase (Liver axial)

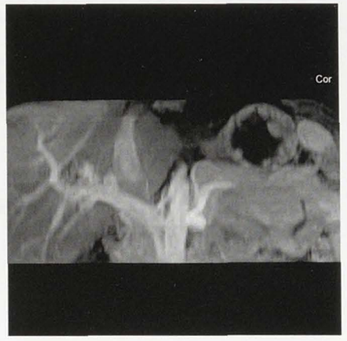

Fig. 5
FLASH 1, 45 sec postGd or recently VIBE 1,45 sec post Gd
(Volume Interpolated Breathhold Examination allowing the examination of the parenchyma and the vasculature with one study)

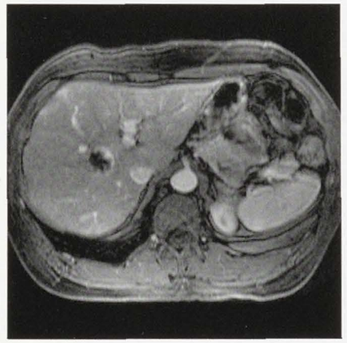

Fig. 6
Fat suppressed FLASH 90 sec postGd or VIBE 90 sec postGd
(Liver, mid abdomen axial)

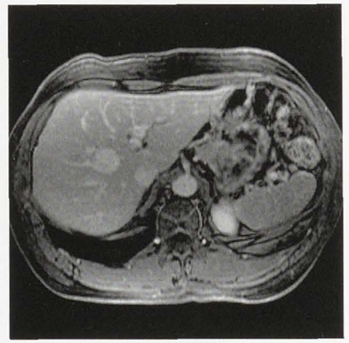

Fig. 7
FLASH 5-min postGd (transverse)

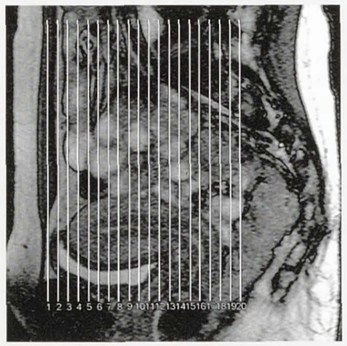

Fig. 8
Localizer (pelvis)

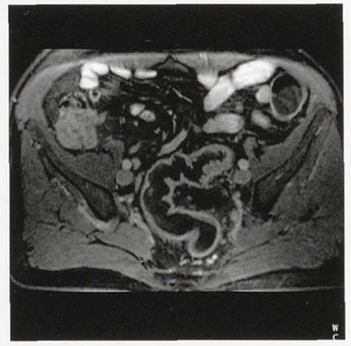

Fig. 9
Fat suppressed FLASH or recently VIBE (axial, sagittal)

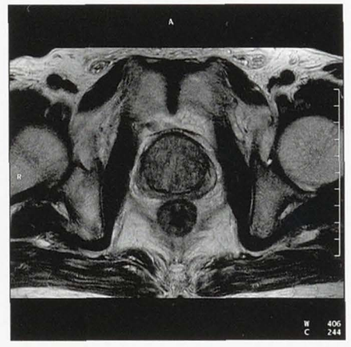

Fig. 10
T_2 high resolution TSE (axial, sagittal)

SiemensMedical.com
Joining the Siemens MR Community – MR Clinics and MAGNETOM World

Nejat Bengi, MD, Siemens Medical Solutions, Erlangen, Germany

The results of the advances in MR technology are numerous new applications that directly affect today's clinical practice. However, our rapidly changing world makes it difficult at times to follow their clinical impact. For this reason we present examplified procedures and their effect on a site's clinical routine and on a patient's diagnostic workup. Examples are collected from various parts of the world.

To bring new applicaitons into the clinical world, Siemens Medical Solutions created the MR Community in the Internet. It is a place where Siemens MAGNETOM users provide clinical case studies in various clinical areas, future views, imaging and application tips to our MR community.

How to get there?

The MR Clinics and MAGNETOM World are linked to the home page of Magnetic Resonance in both the international as well as the German version. In the near future, the US page will include the MR Clinics and MAGNETOM World as well.

You can directly get to the page via: www.siemensmedical.com/mr.

The first time you visit the page you will have to select the international, German or US version.

Now you have the possibility to view the MAGNETOM World or visit the MR Clinics.

Select: MAGNETOM World:

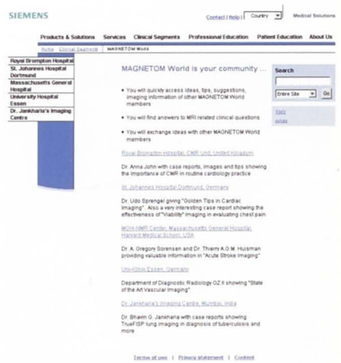

Take a look at the case studies, clinical methods, imaging, tips, or community sites that support selected clinical areas.

At the moment, we provide the following content for MR Clinics and MAGNETOM World

1. Royal Brompton Hospital, United Kingdom: The image gallery includes twenty-seven different cases showing the importance of cardiac MR.
A case study shows that segmented cine TrueFISP increases the diagnostic reliability of MR cine imaging.

2. St. Johannes Hospital, Dortmund, Germany: Cardiac case study shows the importance of Siemens-patented viability technique in diagnosing infarcts. Application tips for optimal use of Cardiac MR Imaging.

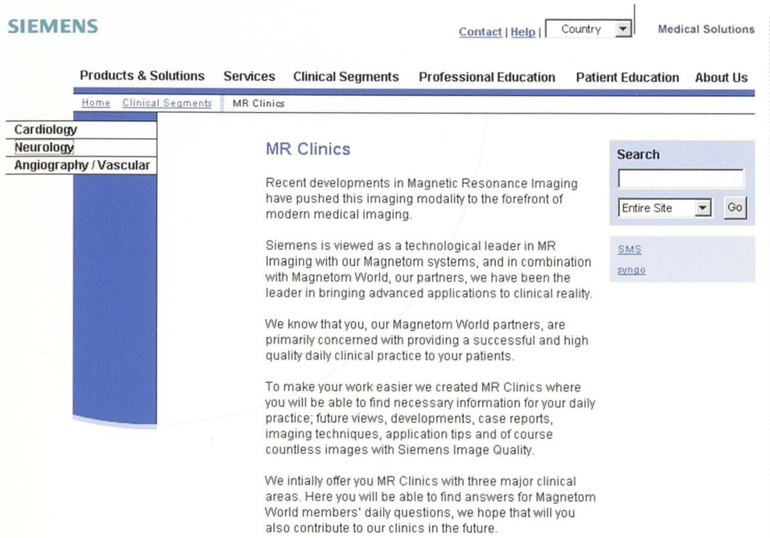

3. Massachusetts General Hospital, Boston, USA: Future views, case reports, application tips, and clinical methods describing new techniques in stroke imaging.

4. University Essen, Germany: Twenty-five angiography studies plus tips are presented, showing how to get the most out of MR angiography techniques.

5. Dr. Jankharia's Imaging Center, Mumbai, India: Case reports showing TrueFISP lung imaging for tubercolosis. Case reports, clinical studies, application tips.

Choosing "MR Clinics" provides three clinical areas at the moment: Cardiology, Neurology and Angiography/Vascular. Selecting one of the areas will provide more detailed information.

We kindly invite you to join the Siemens MR Community at MAGNETOM World and MR Clinics.

Published by

Siemens AG, Medical Solutions
P.O.Box 3260
D-91052 Erlangen

CORRESPONDENCE AND INTERNATIONAL DISTRIBUTION

Dagmar Thomsik-Schroepfer,
PhD, Editor
MAGNETOM FLASH
Siemens AG, Medical Solutions,
Med MRM3
Allee im Röthelheimpark 3
D-91052 Erlangen
Phone: 49 - 91 31 - 84 - 58 73
Fax: 49 - 91 31 - 84 - 21 86

e-mail: dagmar.thomsik-schroepfer@siemens.com

US DISTRIBUTION

Siemens Uptime Service Center
MR Applications
110 MacAlyson Court
Cary, NC 27511
Phone: 800 - 888 - 7436

TECHNICAL EDITOR

Helmuth Schultze-Haakh, PhD
Siemens Medical Systems, Inc
9742 Ravenscroft Road
Santa Ana, CA 92705
Voicemail: 800 - 753 - 63 36, ext 21 17

e-mail: helmuth.schultzehaakh@sms.siemens.com

Internet:
www.siemensmedical.com
www.siemensmedicalacademy.com

Order No. A91100-M2220-E813-4-7600
CC 61813 WS 110120.